Ship motion modeling using an optimized extended state observer-least squares support vector machine

Shuo Xie[a,b,c], Vittorio Garofano[b], Liu Chenguang[a], Xiumin Chu[a], Rudy R. Negenborn[b]

[a]*Intelligent Transportation Systems Research Center, Wuhan University of Technology, 430063, Wuhan, Hubei Province, P.R. China.*
[b]*Department of Maritime and Transport Technology, Delft University of Technology, 2628 CD Delft, The Netherlands*
[c]*School of Energy and Power Engineering, Wuhan University of Technology, 430063, Wuhan, Hubei Province, P.R. China.*

Abstract

Uncertainties including disturbances and non-uniform sampling bring challenges to the accurate modeling of ship motion models. In order to improve the identification performance of the least squares support vector machine (LSSVM) with uncertainties, an extended state observer-LSSVM (ESO-LSSVM) is proposed by using the observations of ESO for continuous system identification. Besides, the ESO-LSSVM is fine-tuned by an adaptive beetle swarm antenna search optimizer (ABSAS-ESO-LSSVM, ABEL) for optimal identification. Identification experiments based on different model ships are conducted to verify the effectiveness of the proposed ABEL method. The identification results indicate that the proposed ABEL method outperforms traditional LSSVM with different levels of disturbances and non-uniform sampling.

Keywords: Parameter identification, ship motion model, support vector machine, extended state observer, beetle swarm antenna search

1. Introduction

With the increasing demand of ship autonomous operation (Zheng et al., 2017, 2018), ship motion modeling methods have been widely studied in recent years. Ship motion has large inertia, nonlinearity, hysteresis and coupling characteristics, which brings challenges to the accurate modeling under uncertain disturbances. Existing ship motion modeling methods involve mechanism modeling and identification modeling (Bai et al., 2019a). Benefiting from easy implementation, the identification modeling methods have attracted more attention recently, which include the parametric modeling and non-parametric modeling methods. The parametric modeling adopts a known structure of ship motion model and the hydrodynamic coefficients are estimated by identification approaches, which is represented by the least squares (LS) (Zhu et al., 2013) and the Kalman filtering (KF) (Fossen et al., 1996; Xie et al., 2019a). The non-parametric modeling is a model structure-agnostic approach that concerns about the response characteristics of the system. Neural networks (NN) (Zhang and Zou, 2013a; Sonnenburg and Woolsey, 2013), support vector machine (SVM) with nonlinear kernels (Hou and Zou, 2015; Hou et al., 2018) and locally weighted learning (LWL) (Bai et al., 2019a, 2018, 2019b) are typical non-parametric modeling methods, which have made great achievements in ship motion modeling. Among these methods, the SVM has a rigorous theoretical basis and considers both structural and empirical risks, which is widely used in ship motion modeling.

Email address: `xieshuo@whut.edu.cn` (Shuo Xie)

In this section, a brief survey of ship motion modeling methods and the related works on SVM based ship model identification are introduced. In the meantime, the related works on the other techniques used in this study, i.e., extended state observer and beetle swarm antenna search, are also introduced.

1.1. A brief survey of ship motion modeling methods

Traditional parametric identification methods, i.e., LS and KF, can identify the ship motion model with a deterministic model structure. LS method estimates the parameters of the model by minimizing the sum square errors, which is widely applied to the identification of the Nomoto model and the Abokwitz model (Zhu et al., 2013). Because of the concise and simple strategy, the LS has a very small amount of computation. In the meantime, LS has a weak fitting ability to the non-linear ship motion model (Luo, 2009), and the identification results of LS are sensitive to the external disturbances. Benefiting from the simultaneous prediction ability of the noise and state, the KF can obtain more accurate results than LS under certain disturbances (Fossen et al., 1996; Xie et al., 2019a), but also requires an appropriate initialization of the noise variance (Haseltine and Rawlings, 2005).

Compared with the parametric identification methods, existing non-parametric identification methods used in ship motion modeling defect the dependency problem on initialization and unmodeled dynamics by function approximation techniques (Bai et al., 2019a). The NN (Sonnenburg and Woolsey, 2013) uses different activation functions and weight matrix to construct a black-box function to approximate the original system. The LWL (Bai et al., 2019a,b) uses piecewise linear models in a neighborhood to approximate the nonlinear functions, of which the size and shape are determined by the distance metric. The SVM (Hou et al., 2018) uses kernel functions to map the original state into a hyper-plane and solves the regression problem easily by minimizing an objective function considering both structural and empirical risks in hyperspace, which has the different representative ability with different kernel functions. Compared with NN, the SVM defects the dimension-disaster problem by the hyper-dimensional space mapping, and avoids the over-fitting problem by minimizing the structural risk, which becomes a mature method for ship motion modeling (Luo, 2009). In addition, the original SVM uses inequality constraints for fitting errors in high-dimensional space, which makes it difficult to solve the optimization problem. As a modified form of SVM, the least squares support vector machine (LSSVM) (Suykens and Vandewalle, 1999) simplifies the inequality constraints in SVM to equality constraints, and the optimization problem is simplified to a solution of linear equations, which reduces the uncertainty of hyper-parameter adjustment.

1.2. Related works on SVM for ship motion modeling

SVM and LSSVM methods have been extensively applied in ship motion model identification in the aspects of both parametric and nonparametric identification, which depends on the type of the kernel function used in SVM.

In the aspect of the non-parametric identification, the ship motion is modeled by the regression model of SVM, which represented by the support vectors, the Lagrange multipliers and the bias. The radial basis function (RBF) kernel is the most commonly used kernel in SVM for non-parametric identification. In (Hou et al., 2018), a non-parametric identification of ship roll motion in irregular waves is realized by a support vector machine with an RBF kernel, which can predict the damping and restoring moments quit well. In (Kawan et al., 2017), the SVM with RBF kernel is used for 3-DOF motion prediction together with a sensitivity analysis, and the accurate prediction of the raw trajectory and pitch data of a ship is realized.

In the aspect of the parametric identification, the ship motion model parameters can be directly obtained by the sum of the support vectors with a linear kernel function, which are weighted by the corresponding Lagrange multipliers. In (Zhang and Zou, 2011), the ϵ-SVM is used for identification modeling of ship motion with a linear kernel function, and the accuracy of the identified hydrodynamics are verified with the planar motion mechanism (PMM) test results. Other similar identification methods based on ϵ-SVM can be found in (Zhang and Zou, 2013b; Wang et al., 2015). Besides, since the LSSVM has less design parameters than the SVM, the linear kernel-based LSSVM is widely used in ship motion model identification recently. In (Luo et al., 2016), the parameter drift of ship motion is diminished by sample reconstruction, and an LSSVM with a linear kernel function is used to identify the parameters in the modified model, which obtains accurate prediction results. Other similar linear kernel-based LSSVM methods can be found in (Luo and Li, 2017; Zhu et al., 2017a).

Although LSSVM has advantages in parametric identification, the hyper-parameter of LSSVM, i.e., the regular factor, still have important impacts on the balance between the structural and empirical risks. To defect this problem, optimization algorithms, e.g., the swarm intelligence (SI) algorithms, are widely used to fine-tune the regular factor of LSSVM, including the particle swarm optimization (PSO) (Luo et al., 2016), the artificial bee colony algorithm (Zhu et al., 2017b), the artificial fish swarm algorithm (Sheng and Na, 2009), the fruit fly optimization algorithm (Li et al., 2016), etc.

In summary, the SVM/LSSVM methods have been mature approaches to identify the ship motion model. By simplifying the conditions in SVM, the LSSVM method reduces the complexity of the identification process.

1.3. Related works on the state observer for identification

State (or disturbance) observers are widely used as elegant approaches to estimate unknown states and disturbances, including the unknown input observer (UIO), the disturbance observer (DOB) the equivalent input disturbance observer (EID) and the extended state observer (ESO). Among them, the ESO requires the least amount of plant information and has the ability to observe the unknown states and disturbances at the same time. During the past decades, ESO has been initially applied to various industrial control systems with disturbances, such as servo system (Pablo et al., 2008; Liu and Li, 2011), robotic system (Su et al., 2004; Cui et al., 2017), ship control system (Liu et al., 2017a; Xie et al., 2019b), electro-hydraulic system (Guo et al., 2016), etc.

With the deepening of research, the state observer has been also applied in system identification problems in recent years. An application of the state observer in identification is to observe unknown states that are difficult to identify. In (Ahmed-Ali et al., 2009) a novel identification method is proposed for time-varying nonlinear systems by integrating a sliding-neural network observer into a simple static parameter estimation law, which obtains good results in numerical cases. In (Bonnabel et al., 2009) a symmetry-preserving observer-based parameter identification algorithm is proposed for quantum systems, which adopts an adaptive observer to observe the atom-laser coupling constants successfully. In (Zhou et al., 2018) a generalized ESO is combined with a recursive least square (RLS) identification method to estimate the state of energy, which provides a better estimation accuracy than the existing methods. In (Xu et al., 2017) ESO is also used to observe the unknown states in a multi-innovation state-delay system, and the multi-innovation identification method is adopted with the states observed by ESO (Ma and Ding, 2015).

In addition, since the continuous states and disturbances can be observed by the state observer, the dependence of system identification on uniform sampling can be defected by using the observed states instead of the original discrete

3

states for identification. (Ikeda et al., 2003) proposes a continuous-time model identification method by using an adaptive state observer, and the theoretical stability of the identification is also proofed. In the aspect of ESO, (Zhang and Han, 2000) uses an state-compensate ESO for the identification of a continuous system, which allows the known dynamics observed by ESO in the system to compensate the estimation of ESO itself.

At present, the ESO has been widely studied in adjustable systems, e.g., the piezoelectric driving system identification (Liu et al., 2017b) and the servo motor control system (Nie et al., 2017). With the combination of traditional identification methods, e.g., the LS method, the ESO has shown the advantages in identification with uncertainties.

1.4. Related works on BSAS for optimization

Stochastic optimization algorithms are widely used for complex optimization problems like hyper-parameter fine-tuning. As a novel branch of stochastic optimization algorithm similar to PSO, the beetle antenna search (BAS) algorithm is proposed in (Jiang and Li, 2018), which has a more concise search strategy. Original BAS algorithm imitates the foraging behavior of beetles and realizes optimization by only one beetle. To deal with more complex problems, beetle swarm antenna search (BSAS) (Wang and Chen, 2018) and beetle swarm optimization (BSO) (Wang et al., 2018) are proposed by combining the advantages of BAS and PSO algorithms. The effectivenesses of BSAS and BSO have been validated in several optimization problems (Sun et al., 2019; Lin et al., 2018; Lin and Li, 2018). (Sun et al., 2019) propose a BAS-based fine-tuning method for the back-propagation neural network (BPNN), which is applied for nonlinear relationship modeling. (Lin et al., 2018) use the BAS algorithm to solve the PID fine-tuning problem of the double closed-loop DC motor speed regulator, which also obtains good fine-tuning performance. (Wu et al., 2019) propose a novel fall-back BAS algorithm for collision-free path planning, which obtains better results compared with original BAS algorithm. In (Xie et al., 2019d), the BSAS algorithm is used to solve the optimization problem for ship collision avoidance, which also obtains effective results.

Due to the concise search strategy, BAS and BSAS-based algorithms have great potential for difficult hyper-parameter fine-tuning problems.

1.5. Motivations and contributions

Although various identification methods have been studied, accurate ship motion modeling with uncertain disturbances and non-uniform sampling is still difficult since most of the existing ship modeling methods are discrete methods. Since the ESO can observe continuous higher-order states and the LSSVM can minimize the structural risks caused by over-fitting, a novel ESO-LSSVM scheme is proposed based on LSSVM and ESO to defect the above problems. Besides, the hyper-parameters of ESO-LSSVM are fine-tuned adaptively by a BSAS optimizer to form the final ABEL method. To the best of our knowledge, the combination of ESO and LSSVM has seldom been studied for ship motion modeling. The main contributions of this study are briefly summarized as follows:

1) Compared with existing LSSVM identification methods for ship motion model, an ESO is integrated in LSSVM to deal with uncertain disturbances and non-uniform sampling.

2) To obtain the optimal performance of the proposed ESO-LSSVM scheme, an adaptive BSAS optimizer is used for fine-tuning of the hyper-parameters of ESO.

1.6. Outlines

The remainder of this article is organized as follows. In Section 2, the traditional LSSVM identification method is introduced for ship motion model. In Section 3, the ABEL identification method is proposed for identification

4

with uncertainties. In Section 4, case studies are conducted based on the widely used KVLCC2 model ship, a novel fully-actuated Delfia 1* ship and a real Tito-Neri tug ship to verify the identification modeling performance of the proposed ABEL method. In Section 5, conclusions and further works are presented.

2. Traditional LSSVM method for ship motion model identification

LSSVM is a widely used regression method for ship motion modeling, which linearizes the traditional SVM method by transforming the inequality constraints into equality conditions. In this section, the traditional LSSVM method for ship motion model identification is denoted.

2.1. Ship motion model

Generally, the surface ship motion can be simplified to 3 degree-of-freedom (DOF) as shown in Fig. 1. Where $O_o - x_o y_o$ is the inertial coordinate system of the ship; $O - xy$ is the co-rotational coordinate system of the ship; $u(t)$, $v(t)$ and $r(t)$ are the velocities in surge (body-fixed x), sway (body-fixed y) and yaw directions, respectively, m(rad)/s; $\delta(t)$ and $\psi(t)$ are the rudder and heading angle of the vessel, respectively, rad; $\beta(t)$ is the drift angle, rad.
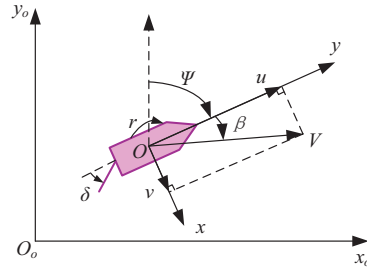

Figure 1: Ship motion coordinate system.

Then the ship motion model is established by the kinematic model and hydrodynamic model. The kinematic model describes the relationship between the ship positions in the inertial coordinate system $O_o - x_o y_o$ and the velocities in the co-rotational coordinate system $O - xy$. The hydrodynamic model describes the relationship between the hydrodynamic forces (moments) and the 3-DOF ship motions, of which the hydrodynamic parameters need to be identified.

1) The kinematic model

Based on geometric decompositions, the kinematic model of a surface ship is obtained by a rotation matrix:

$$\dot{\boldsymbol{\eta}}(t) = \boldsymbol{R}(\psi(t))\boldsymbol{v}(t), \boldsymbol{R}(\psi(t)) = \begin{bmatrix} \sin(\psi(t)) & \cos(\psi(t)) & 0 \\ -\cos(\psi(t)) & \sin(\psi(t)) & 0 \\ 0 & 0 & 1 \end{bmatrix}, \tag{1}$$

where $\boldsymbol{\eta}(t) = \begin{bmatrix} x(t) & y(t) & \psi(t) \end{bmatrix}^{\mathrm{T}}$ and $\boldsymbol{v}(t) = \begin{bmatrix} u(t) & v(t) & r(t) \end{bmatrix}^{\mathrm{T}}$ are the position and velocity vectors of the ship, respectively; $\boldsymbol{R}(\psi(t))$ is the rotation matrix.

2) The hydrodynamic model

Abkowitz model (Abkowitz, 1980) and MMG (math model group) model (Yasukawa and Yoshimura, 2015) are the most widely used hydrodynamic models. The Abokwitz model takes the Taylor expansion coefficients of the

5

3-DOF forces (moments) with respect to different motion states as the hydrodynamic parameters. While the MMG model can be regarded as a simplification of Abokwitz model by separating the forces from aspects of the hull, the rudder and the propeller. Generally, the dynamic equation of the Abokwitz model is:

$$\boldsymbol{M}\dot{\boldsymbol{v}}(t) = \boldsymbol{f}(u(t), v(t), r(t), \delta(t), n(t)), \tag{2}$$

where $\delta(t)$ is the rudder angle and $n(t)$ is the engine speed, r/min; $\boldsymbol{f}$ is the nonlinear lumped force and moment matrix of the ship with respect to $\boldsymbol{v}(t), \delta(t)$ and $n(t)$; $\boldsymbol{M}$ is the inertia matrix of the ship:

$$\boldsymbol{M} = \begin{bmatrix} m - X_{\dot{u}} & 0 & 0 \\ 0 & m - Y_{\dot{v}} & mx_G - Y_{\dot{r}} \\ 0 & mx_G - N_{\dot{v}} & I_z - N_{\dot{r}} \end{bmatrix}, \tag{3}$$

where m is the total mass of the vessel, kg; x_G is the longitudinal coordinate of the gravity center of the vessel in surge direction, m; I_Z is the moment of the inertia, kg·m^2; $X_{\dot{u}}, Y_{\dot{v}}, Y_{\dot{r}}, N_{\dot{v}}$ and $N_{\dot{r}}$ are the inertia coefficients. Using $\Delta u(t) = u(t) - u_0$, $\Delta v(t) = v(t) - v_0$ and $\Delta r(t) = r(t) - r_0$ represent the perturbations from the constant surge speed u_0, sway speed v_0 and yaw speed r_0, respectively, the ship motion model can be re-written as:

$$\Delta\dot{u}(t) = \Delta f_u(t) / (m - X_{\dot{u}}),$$
$$\Delta\dot{v}(t) = [(I_Z - N_{\dot{r}})\Delta f_v(t) - (mx_G - Y_{\dot{r}})\Delta f_r(t)] / (I_Z - N_{\dot{r}})(m - Y_{\dot{v}}) - (mx_G - Y_{\dot{r}})(mx_G - N_{\dot{v}}), \tag{4}$$
$$\Delta\dot{r}(t) = [(m - Y_{\dot{v}})\Delta f_r(t) - (mx_G - N_{\dot{v}})\Delta f_v(t)] / (I_Z - N_{\dot{r}})(m - Y_{\dot{v}}) - (mx_G - Y_{\dot{r}})(mx_G - N_{\dot{v}}),$$

where $\Delta f_u(t)$, $\Delta f_v(t)$ and $\Delta f_r(t)$ are the force and moment components of $\boldsymbol{f}$ at time t in surge, sway and yaw directions, respectively. After considering the disturbances, the 3-DOF ship motion model can be re-written as the following parameter-linearized model:

$$\begin{bmatrix} \Delta\dot{u}(t) \\ \Delta\dot{v}(t) \\ \Delta\dot{r}(t) \end{bmatrix} = \begin{bmatrix} \boldsymbol{\Theta}_u & \boldsymbol{0} & \boldsymbol{0} \\ \boldsymbol{0} & \boldsymbol{\Theta}_v & \boldsymbol{0} \\ \boldsymbol{0} & \boldsymbol{0} & \boldsymbol{\Theta}_r \end{bmatrix}^{\mathrm{T}} \begin{bmatrix} \boldsymbol{S}_u(t) \\ \boldsymbol{S}_v(t) \\ \boldsymbol{S}_r(t) \end{bmatrix} + \begin{bmatrix} d_u(t) \\ d_v(t) \\ d_r(t) \end{bmatrix}, \tag{5}$$

where $\boldsymbol{d}(t) = \begin{bmatrix} d_u(t) & d_v(t) & d_r(t) \end{bmatrix}^{\mathrm{T}} \in \mathbb{R}^{3\times 1}$ is the disturbance vector in 3-DOF; $\boldsymbol{\Theta}_u, \boldsymbol{\Theta}_v$ and $\boldsymbol{\Theta}_r$ are the parameter vectors to be identified in 3-DOF; $\boldsymbol{S}_u(t), \boldsymbol{S}_v(t), \boldsymbol{S}_r(t)$ are the state information matrices which are defined by the dimensional state variables with non-dimensional coefficients in Taylor's expansions of Δf_u, Δf_v and Δf_r respectively (Luo, 2009):

$$\boldsymbol{S}_u(t) = [\Delta u(t), \Delta u(t)U(t), \Delta u^2(t), \Delta u^3(t)/U(t), \Delta v^2(t), \Delta r^2(t), \Delta\delta^2(t)U^2(t),$$
$$\Delta\delta^2(t)\Delta u(t)U(t), \Delta v(t)\Delta r(t), \Delta v(t)\Delta\delta(t)U(t)]^{\mathrm{T}}_{11\times 1},$$

$$\boldsymbol{S}_v(t) = [\Delta v(t), U^2(t), \Delta u(t)U(t), \Delta u^2(t), \Delta v(t)U(t), \Delta r(t)U(t), \Delta\delta(t)U^2(t),$$
$$\Delta v^3(t)/U(t), \Delta\delta^3(t)U^2(t), \Delta v^2(t)\Delta r(t)/U(t), \Delta v^2(t)\Delta\delta(t), \Delta v(k)\Delta\delta^2(t)U(t),$$
$$\Delta\delta(t)\Delta u(t)U(t), \Delta v(t)\Delta u(t), \Delta r(t)\Delta u(t), \Delta\delta(t)\Delta u^2(t)]^{\mathrm{T}}_{16\times 1}, \tag{6}$$

$$\boldsymbol{S}_r(t) = [\Delta r(t), U^2(t), \Delta u(t)U(t), \Delta u^2(t), \Delta v(t)U(t), \Delta r(t)U(t), \Delta\delta(t)U^2(t),$$
$$\Delta v^3(t)/U(t), \Delta\delta^3(t)U^2(t), \Delta v^2(t)\Delta r(t)/U(t), \Delta v^2(t)\Delta\delta(t), \Delta v(k)\Delta\delta^2(t)U(t),$$
$$\Delta\delta(t)\Delta u(t)U(t), \Delta v(t)\Delta u(t), \Delta r(t)\Delta u(t), \Delta\delta(t)\Delta u^2(t)]^{\mathrm{T}}_{16\times 1},$$

where $U(t) = \sqrt{u(t)^2 + v(t)^2}$ is the speed of the ship.

6

2.2. LSSVM identification

Assuming that the state matrices $\mathbf{S}_u(t)$, $\mathbf{S}_v(t)$, $\mathbf{S}_r(t)$ are measurable, the parameter vector in each DOF can be identified by LSSVM separately. Take the parameter $\mathbf{\Theta}_r$ in (5) in the yaw direction as an example. Considering a data set of which a point represented by $\{\mathbf{x}_k, y_k\}_{k=1}^l$ where $\mathbf{x}_k \sim \mathbf{S}_r$ is the kth input data and $y_k(\mathbf{x}_k) \sim \Delta \dot{r}$ is the output data with respect to $\mathbf{x}_k$, l is the data size. The LSSVM method uses a regression model represented by a hyper-plane to modeling the data set:

$$y = f(\mathbf{x}) = \mathbf{w} \cdot \boldsymbol{\phi}(\mathbf{x}) + b, \tag{7}$$

where $\boldsymbol{\phi}(\cdot)$ is the kernel function that maps the input $\mathbf{x}$ into a higher dimensional space; $\mathbf{w}$ is the weighting vector in the higher dimensional space; b is the bias. Then $\mathbf{w}$ and b are obtained by minimizing the objective function as follows:

$$\min_{\mathbf{w}, b, \xi} J(\mathbf{w}, b, \xi) = \left\{ \tfrac{1}{2} \mathbf{w}^T \mathbf{w} + \tfrac{1}{2} C \sum_{i=1}^l \xi_i^2 \right\},$$
$$s.t. \quad y_i - [\mathbf{w}^T \boldsymbol{\phi}(\mathbf{x}_i) + b] = \xi_i, \tag{8}$$

where ξ is the fitting error and C is the regular factor for punishing the fitting error. Then a Lagrange function is established for solving Eq. (8) as:

$$L(\mathbf{w}, b, \xi, \alpha) = \frac{1}{2} \mathbf{w}^T \mathbf{w} + \frac{1}{2} C \sum_{i=1}^l \left(\xi_i^2 \right) - \sum_{i=1}^l \alpha_i \left[\xi_i - y_i + \mathbf{w}^T \boldsymbol{\phi}(\mathbf{x}_i) + b \right], \tag{9}$$

where l is the size of the data set; α_i is the Lagrange multiplier with respect to the constraint of the point $\{\mathbf{x}_i, y_i\}$. To minimize the function $L(\mathbf{w}, b, \xi, \alpha)$, the following KKT conditions are given by the partial derivations:

$$\begin{cases} \frac{\partial L}{\partial \mathbf{w}} = 0 \\ \frac{\partial L}{\partial b} = 0 \\ \frac{\partial L}{\partial \xi_i} = 0 \\ \frac{\partial L}{\partial \alpha_i} = 0 \end{cases} \Rightarrow \begin{cases} \mathbf{w} = \sum_{i=1}^l \alpha_i \boldsymbol{\phi}(\mathbf{x}_i) \\ \sum_{i=1}^l \alpha_i = 0 \\ C \cdot \xi_i = \alpha_i \\ \mathbf{w}^T \boldsymbol{\phi}(\mathbf{x}_i) + b + \xi_i - y_i = 0 \end{cases}. \tag{10}$$

Therefore, the Lagrange multiplier α_i and bias b can be obtained by solving the following linear system of equations:

$$\begin{bmatrix} 0 & \mathbf{1}_{1 \times l} \\ \mathbf{1}_{l \times 1} & \mathbf{\Omega}_{l \times l} \end{bmatrix} \begin{bmatrix} b \\ \boldsymbol{\alpha}_{l \times 1} \end{bmatrix} = \begin{bmatrix} 0 \\ \mathbf{y}_{l \times 1} \end{bmatrix}, \mathbf{\Omega}_{l \times l} = \begin{bmatrix} K(\mathbf{x}_1, \mathbf{x}_1) & \cdots & K(\mathbf{x}_1, \mathbf{x}_l) \\ \vdots & \ddots & \vdots \\ K(\mathbf{x}_l, \mathbf{x}_1) & \cdots & K(\mathbf{x}_l, \mathbf{x}_l) \end{bmatrix}_{l \times l} + \tfrac{1}{C} \cdot \mathbf{I}_{l \times l}, \tag{11}$$

$$\boldsymbol{\alpha}_{l \times 1} = \begin{bmatrix} \alpha_1 & \alpha_2 & \cdots & \alpha_l \end{bmatrix}^T, \mathbf{y}_{l \times 1} = \begin{bmatrix} y_1 & y_2 & \cdots & y_l \end{bmatrix}^T,$$

where $K(\mathbf{x}_i, \mathbf{x}_j) = \boldsymbol{\phi}(\mathbf{x}_i) \cdot \boldsymbol{\phi}(\mathbf{x}_j)$ is the kernel function which satisfies the Mercer's condition. Then, the regression model of LSSVM is obtained as:

$$y = \sum_{i=1}^l \alpha_i \phi(\mathbf{x}_i) \cdot \boldsymbol{\phi}(\mathbf{x}) + b = \sum_{i=1}^l \alpha_i K(\mathbf{x}_i, \mathbf{x}) + b. \tag{12}$$

According to different modeling requirements, appropriate kernel function should be selected for regression or parameter identification, e.g., linear kernel, RBF(radial basis function) kernel and polynomial kernel, etc. Considering the parameter-linearized model (5), the following linear kernel is used for the identification:

$$K(\mathbf{x}_i, \mathbf{x}_j) = \mathbf{x}_i^T \mathbf{x}_j. \tag{13}$$

Then the LSSVM regression model in yaw direction can be obtained as $y = \sum_{i=1}^{l} \alpha_i(x_i) \cdot x + b$ if the bias $b \to 0$. The parameter matrix Θ_r can be identified as:

$$\Theta_r = \sum_{i=1}^{l} \alpha_i(x_i). \tag{14}$$

Finally, the other parameter matrices Θ_u and Θ_v in (5) can be identified based on LSSVM similarly to establish the complete hydrodynamic model.

3. The proposed ABEL method

Due to the uncertainties including disturbances and non-uniform sampling, the measurement accuracy of ship states is seriously affected, resulting in inaccurate higher-order states (i.e., the surge, sway, and yaw accelerations). To defect this problem, an extended state observer is designed to observe the continuous higher-order states for combination with LSSVM in this section. Furthermore, an adaptive beetle swarm antenna search (ABSAS) algorithm is used to fine-tune the hyper-parameters of the designed ESO. Methodologies are illustrated in two subsections: the ESO-LSSVM identification scheme and the proposed ABEL (ABSAS-optimized ESO-LSSVM) method.

3.1. ESO-LSSVM identification scheme

For standardization, the 3-DOF ship motion model (5) is represented by the following classic parameter-linearized model with n-dimensions in the following statement:

$$\begin{cases} \dot{x} = \Theta S(x, u) + d, \\ y = Cx, \end{cases} \tag{15}$$

where $x \in \mathbb{R}^{n \times 1}$ is the state vector, n is the dimension of x; u is the system input; $S(x, u) \in \mathbb{R}^{m \times 1}$ is the state information vector consisting of the state x and system input u, m is the dimension of $S(x, u)$; $\Theta \in \mathbb{R}^{n \times m}$ is the parameter vector to be identified; $d \in \mathbb{R}^{n \times 1}$ is the disturbance vector; $y \in \mathbb{R}$ is the output and $C \in \mathbb{R}^{1 \times n}$ is the measuring matrix. Then, the proposed ESO-LSSVM scheme for (15) is shown in Fig. 2, which includes two main parts: the ESO designing and continuous LSSVM identification.

3.1.1. ESO designing for higher-order state observations

The ESO has been widely used to observe the lumped disturbances and high-order states for adaptive control (Liu et al., 2017a, 2008). Assuming that the matrix C and the state information vector $S(x, u)$ are known, the target of the identification for model (15) is to determine the parameter matrix Θ. In order to generate accurate continuous higher-order states $\dot{x}$ for LSSVM, an ESO is designed by defining the entire term with respect to the parameter matrix $\Theta S(x, u)$ and the disturbances d as the equivalent disturbances :

$$d_E = \dot{x} = \Theta S(x, u) + d, \tag{16}$$

where d_E is the equivalent disturbance matrix. Then another extended state vector is defined as the derivative of the equivalent disturbance $\dot{d}_E$, the state vectors of the system (15) are re-defined as $\beta = \begin{bmatrix} x & d_E & \dot{d}_E \end{bmatrix}^{\mathrm{T}}_{3n \times 1}$ and the whole system is re-written as:

$$\begin{cases} \dot{\beta} = A\beta + Eh, \\ y = D\beta, \end{cases} \tag{17}$$

8
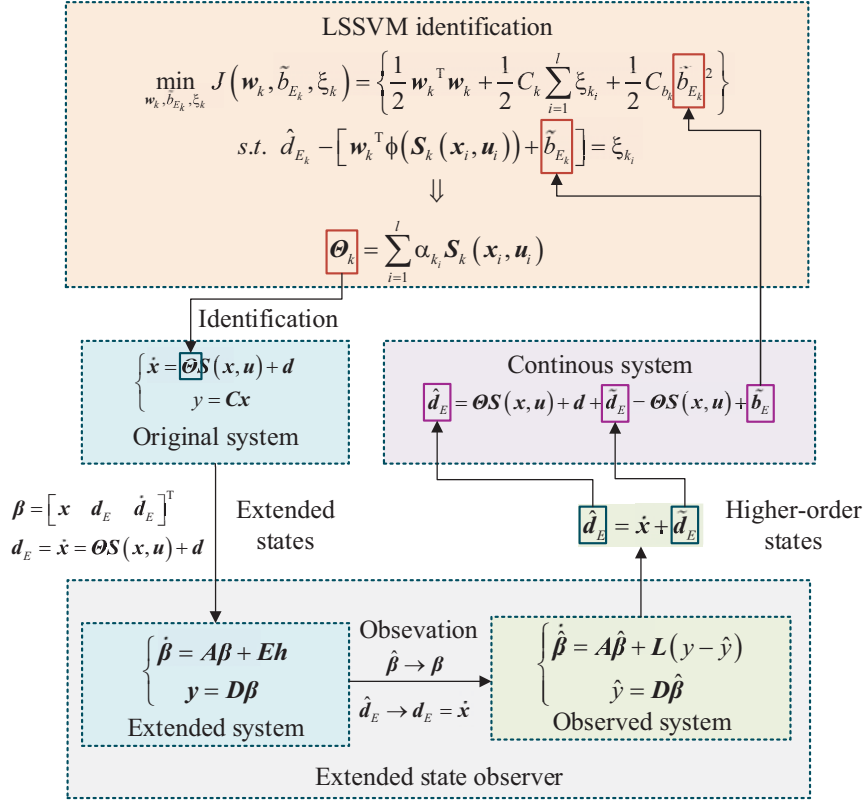
Figure 2: The ESO-LSSVM scheme.

where $\boldsymbol{h} = \ddot{\boldsymbol{d}}_{En \times 1}$ is the 2nd derivation of $\boldsymbol{d}_E$; the matrices $\boldsymbol{A}$, $\boldsymbol{E}$ and $\boldsymbol{D}$ are denoted as:

$$\boldsymbol{A} = \begin{bmatrix} 0_{n \times n} & 1_{n \times n} & 0_{n \times n} \\ 0_{n \times n} & 0_{n \times n} & 1_{n \times n} \\ 0_{n \times n} & 0_{n \times n} & 0_{n \times n} \end{bmatrix}, \boldsymbol{E} = \begin{bmatrix} 0_{n \times 1} & 0_{n \times 1} & 1_{n \times 1} \end{bmatrix}^{\mathrm{T}}, \boldsymbol{D} = \begin{bmatrix} \boldsymbol{C}_{1 \times n} & 0_{n \times 1} & 0_{n \times 1} \end{bmatrix}^{\mathrm{T}}. \tag{18}$$

For system (18), the ESO is designed as follows to observer the high-order states:

$$\begin{cases} \dot{\hat{\boldsymbol{\beta}}} = \boldsymbol{A}\hat{\boldsymbol{\beta}} + \boldsymbol{L}(y - \hat{y}), \\ \hat{y} = \boldsymbol{D}\hat{\boldsymbol{\beta}}, \end{cases} \tag{19}$$

where $\hat{\boldsymbol{\beta}} = \begin{bmatrix} \hat{\boldsymbol{x}} & \hat{\boldsymbol{d}}_E & \hat{\hat{\boldsymbol{d}}}_E \end{bmatrix}^{\mathrm{T}}_{3n \times 1}$ is the observation of $\boldsymbol{\beta}$; $\boldsymbol{L}_{3n \times 1} = \begin{bmatrix} l^1_{n \times 1} & l^2_{n \times 1} & l^3_{n \times 1} \end{bmatrix}^{\mathrm{T}}$ is the observer gain matrix to be designed, where $l^1_{n \times 1}$, $l^2_{n \times 1}$ and $l^3_{n \times 1}$ are the gain vectors with respect to the state $\boldsymbol{x}$, $\boldsymbol{d}_E$ and $\hat{\boldsymbol{d}}_E$, respectively. In addition, the observer gains can be set based on the bandwidth selection approach in ESO (Shao and Wang, 2015; Gao, 2006) as:

$$\begin{aligned} l^1_{n \times 1} &= \begin{bmatrix} 3\omega_1 & 3\omega_2 & \cdots & 3\omega_n \end{bmatrix}^{\mathrm{T}}_{n \times 1}, \\ l^2_{n \times 1} &= \begin{bmatrix} 3\omega_1^2 & 3\omega_2^2 & \cdots & 3\omega_n^2 \end{bmatrix}^{\mathrm{T}}_{n \times 1}, \\ l^3_{n \times 1} &= \begin{bmatrix} \omega_1^3 & \omega_2^3 & \cdots & \omega_n^3 \end{bmatrix}^{\mathrm{T}}_{n \times 1}, \end{aligned} \tag{20}$$

where $\omega_1, \ldots \omega_n$ are the n-dimensional bandwidths. By selecting appropriate bandwidths $\omega = [\omega_1, \ldots \omega_n]$, the observed values of the states in Eq. (24) can be quickly approximated to the higher-order states:

$$\hat{\beta} \to \beta \Rightarrow \begin{cases} \hat{x} \to x, \\ \hat{d}_E \to d_E = \dot{x}, \\ \hat{\dot{d}}_E \to \dot{d}_E. \end{cases} \tag{21}$$

3.1.2. Continuous LSSVM identification

Due to the difficulties of accurate measurement of higher-order states, traditional identification methods usually discrete the continuous model by using the state differences to approximate the differential quantities. The forward difference approximate method is widely applied for identification as:

$$\dot{x}(t) = \frac{1}{h} (x(t+1) - x(t)), \tag{22}$$

where h is the difference interval. Besides the uncertain disturbances, the nonuniform sampling also has influences on the identification accuracy if the actual sampling interval is unstable, or becomes quite different from the setting interval h.

Considering that the established ESO can observe the high-order states continuously, the approximate values $\hat{d}_E$ in ESO are used instead of the forward difference. Assuming that the observe error of the high-order state matrix is $\tilde{d}_E = \hat{d}_E - \dot{x}$, a continuous parameter-linearized system is obtained by combing Eq. (16) and Eq. (21):

$$\hat{d}_E = \dot{x} + \tilde{d}_E = \Theta S(x, u) + d + \tilde{d}_E = \Theta S(x, u) + \tilde{b}_E, \tag{23}$$

where $\tilde{b}_E = d + \tilde{d}_E$ is a lumped equivalent bias vector which aggregates the disturbance d and the observation error $\tilde{d}_E$. Therefore, the parameter matrix Θ can be identified based on LSSVM identification method denoted in the Preliminary section under the following condition:

$$d + \tilde{d}_E \to 0. \tag{24}$$

In order to satisfy the upper condition and realize the unbiased identification as much as possible, a n-dimensional regular vector $C_b = \begin{bmatrix} C_{b_1} & C_{b_2} & \cdots & C_{b_n} \end{bmatrix}_{n \times 1}^{\mathrm{T}}$ with respect to the equivalent bias $\tilde{b}_E$ are added in the objective function of LSSVM as:

$$\min_{w_k, \tilde{b}_{E_k}, \xi_k} J\left(w_k, \tilde{b}_{E_k}, \xi_k\right) = \left\{ \frac{1}{2} w_k^{\mathrm{T}} w_k + \frac{1}{2} C_k \sum_{i=1}^{l} \xi_{k_i} + \frac{1}{2} C_{b_k} \tilde{b}_{E_k}^2 \right\},$$
$$s.t. \quad \hat{d}_{E_k} - \left[w_k^{\mathrm{T}} \phi(S_k(x_i, u_i)) + \tilde{b}_{E_k} \right] = \xi_{k_i}, \tag{25}$$

where $w_k, \tilde{b}_{E_k}, \xi_k, \hat{d}_{E_k}, C_k$ and C_{b_k} are the kth dimension values of the weighting vector w, the equivalent bias $\tilde{b}_E$, the fitting error ξ, the regular factors C and C_d, respectively. Then the Lagrange function and the final linear equations need to be modified correspondingly:

$$L_k(w_k, \hat{d}_{E_k}, \xi_k, \alpha_k) = \frac{1}{2} w_k^{\mathrm{T}} w_k + \frac{1}{2} C_k \sum_{i=1}^{l} \xi_{k_i}^2 + \frac{1}{2} C_{b_k} \tilde{b}_{E_k}^2 - \sum_{i=1}^{l} \alpha_{k_i} \left[\xi_{k_i} - \hat{d}_{E_{k_i}} + w_k^{\mathrm{T}} \phi(S_k(x_i, u_i)) + \tilde{b}_{E_k} \right]. \tag{26}$$

Then, the KKT conditions are modified to:

$$\begin{cases} \frac{\partial L_k}{\partial \boldsymbol{w}_k} = 0 \\ \frac{\partial L_k}{\partial \tilde{b}_{E_k}} = 0 \\ \frac{\partial L_k}{\partial \xi_{k_i}} = 0 \\ \frac{\partial L_k}{\partial \alpha_{k_i}} = 0 \end{cases} \Rightarrow \begin{cases} \boldsymbol{w}_k = \sum\limits_{i=1}^{l} \alpha_{k_i} \phi(\boldsymbol{S}_k(\boldsymbol{x}_i, \boldsymbol{u}_i)) \\ \sum\limits_{i=1}^{l} \alpha_{k_i} = C_{b_k} \tilde{b}_{E_k} \\ C_k \cdot \xi_{k_i} = \alpha_i \\ \boldsymbol{w}_k^{\mathrm{T}} \boldsymbol{S}_k(\boldsymbol{x}_i, \boldsymbol{u}_i) + \tilde{b}_{E_k} + \xi_{k_i} - \hat{d}_{E_{k_i}} = 0 \end{cases}, \tag{27}$$

and the linear system of the LSSVM equations are given by:

$$\begin{bmatrix} -C_{b_k} & \boldsymbol{1}_{1\times l} \\ \boldsymbol{1}_{l\times 1} & \boldsymbol{\Omega}_{l\times l} \end{bmatrix} \begin{bmatrix} \tilde{b}_{E_k} \\ \boldsymbol{\alpha}_{kl} \end{bmatrix} = \begin{bmatrix} 0 \\ \hat{\boldsymbol{d}}_{El} \end{bmatrix}, \tag{28}$$

where $\boldsymbol{\alpha}_{kl} = \begin{bmatrix} \alpha_{k_1} & \alpha_{k_2} & \cdots & \alpha_{k_l} \end{bmatrix}^{\mathrm{T}}_{l\times 1}$, $\hat{\boldsymbol{d}}_{El} = \begin{bmatrix} \hat{d}_{E_{k_1}} & \hat{d}_{E_{k_2}} & \cdots & \hat{d}_{E_{kl}} \end{bmatrix}^{\mathrm{T}}_{l\times 1}$. Then the parameter matrix in k^{th} dimension $\boldsymbol{\Theta}_k = \sum\limits_{i=1}^{l} \alpha_{ki}(\boldsymbol{S}_k(\boldsymbol{x}_i, \boldsymbol{u}_i))$ can be obtained by solving Eq. (28), so as to identify the whole parameter matrix $\boldsymbol{\Theta}$.

In summary, the main differences between the traditional LSSVM and the proposed ESO-LSSVM are as follows:

1) To deal with nonuniform sampling problems, the higher-order states observed by ESO are used in LSSVM for continuous identification.

2) To deal with disturbances, a regular factor with respect to the equivalent bias, which is composed of the ESO observation errors and the disturbances, is introduced in LSSVM to achieve unbiased identification.

3.2. The ABEL method

Although the LSSVM is improved in ESO-LSSVM by adding a regular factor on the equivalent bias, the hyper-parameters of ESO, i.e., the bandwidths, still have great influences on the observation. If inappropriate bandwidths $\omega = [\omega_1, \ldots \omega_n]$ are selected, under-fitting or over-fitting problems will occur in the observation. Then the unbiased identification, i.e., the equivalent bias $\tilde{\boldsymbol{b}}_E \rightarrow \boldsymbol{0}$, is difficult to be satisfied. In this section, an adaptive beetle swarm antenna search (ABSAS) algorithm is used to to adaptively fine-tune the bandwidths ω in ESO-LSSVM. The work flow of the proposed ABEL method is shown in Fig. 3. In each optimization iteration, the updated bandwidths ω are used for ESO-LSSVM identification, and the identified model is applied for state prediction and fitness calculation. Then the ABSAS optimizer updates the ω based on the fitness results until the maximum iteration number or a set fitness threshold is reached.

For ship motion model identification, the dimension $n = 3$ and the bandwidths $\omega = [\omega_1, \omega_2, \omega_3]$ are the hyper-parameters to be optimized. The fitness function $f(\omega)$ can be calculated by the mean squares errors of the ship state predictions in 3-DOF:

$$f(\omega) = R_u + R_v + R_r,$$
$$R_u = \frac{1}{l_{va}} \sum\limits_{i=1}^{l_{va}} \left(u_i^p - u_i^{va} \right)^2, R_v = \frac{1}{l_{va}} \sum\limits_{i=1}^{l_{va}} \left(v_i^p - v_i^{va} \right)^2, R_r = \frac{1}{l_{va}} \sum\limits_{i=1}^{l_{va}} \left(r_i^p - r_i^{va} \right)^2, \tag{29}$$

where $f(\omega)$ is the fitness function; l_{va} is the size of the validation data set; u_i^{va}, v_i^{va} and r_i^{va} are the ith 3-DOF states in the validation data set; u_i^p, v_i^p and r_i^p are the ith surge, sway and yaw velocities predicted by the identified ship model with respect to ω.
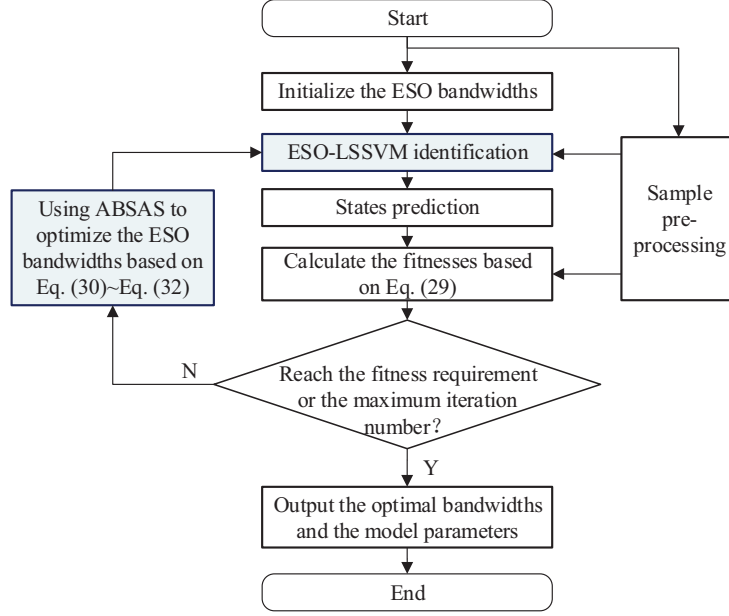
11

Figure 3: The ABEL work flow.

As a branch of the optimization algorithms, the original BSAS algorithm (Wang and Chen, 2018) sets a certain number of beetles to search the optimal parameters for optimization. Further researches (Xie et al., 2019d,c) have proposed an adaptive strategy for BSAS by re-using the historical optimums. Each beetle in the adaptive BSAS searches the optimal parameters based on the following strategy (Xie et al., 2019d):

$$
\begin{aligned}
&\omega_{il}^k = \omega_{ilo} + s_i^k \frac{d}{\|d\|}, \\
&\omega_{ir}^k = \omega_{iro} - s_i^k \frac{d}{\|d\|}, \\
&\begin{cases} f(\omega_{ilo}) = f(\omega_{il}^k), \omega_{ilo} = \omega_{il}^k & if \left\{ f(\omega_{il}^k) < f(\omega_{ilo}) \right\}, \\ f(\omega_{iro}) = f(\omega_{ir}^k), \omega_{iro} = \omega_{ir}^k & if \left\{ f(\omega_{ir}^k) < f(\omega_{iro}) \right\}, \end{cases}
\end{aligned}
\tag{30}
$$

where ω_{il}^k and ω_{ir}^k are the left and right antenna of the ith beetle at k iteration, respectively; s^k is the exploring step of the antennas at k iteration; d is a random vector distributed in $[-1, 1]$ with the same dimension of ω; ω_{ilo} and ω_{iro} are the historical optimums of the left and right antennas, respectively; $f(\omega_{ilo})$ and $f(\omega_{iro})$ are the corresponding historical optimal fitness. Then the update strategy of the beetle centroid is denoted as:

$$
\begin{aligned}
&\omega_i^k = \omega_i^{k-1} + r\lambda_l \left(\omega_{ilo} - \omega_i^{k-1} \right) + r\lambda_r \left(\omega_{iro} - \omega_i^{k-1} \right), \\
&\lambda_l = c \frac{e^{f(\omega_{iro})}}{e^{f(\omega_{ilo})} + e^{f(\omega_{iro})}}, \lambda_r = c - \lambda_l,
\end{aligned}
\tag{31}
$$

where ω_i^k is the centroid of the ith beetle at k iteration; $r \in [0, 1]$ is a random value; λ_l and λ_r are learning factors of the left and right antenna historical optimum, respectively; c is a constant. By learning from two antennas based on the historical optimal fitnesses, the centroid of the beetle gradually approaches the antenna that has better historical performance.

After all beetles finish searching in each iteration, the global and local optimums ω_g, ω_{ibest} and the corresponding

12

fitnesses f_g, $f_{i\text{best}}$ of the beetle swarm are updated by the greedy-policy:

$$\begin{cases} f_{ibest} = f(\boldsymbol{\omega}_i^k), \boldsymbol{\omega}_{ibest} = \boldsymbol{\omega}_i^k & if \left\{ f(\boldsymbol{\omega}_i^k) < f_{ibest} \right\}, \\ f_g = f_{ibest}, \boldsymbol{\omega}_g = \boldsymbol{\omega}_{ibest} & if \left\{ f_{ibest} < f_g \right\}. \end{cases} \tag{32}$$

In addition, to guarantee the global optimality of the algorithm, the left and right historical optimal positions are initialized with the upper and lower bounds of the search space as:
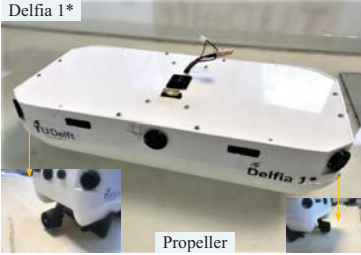
$$\boldsymbol{\omega}_{ilo} \underset{k=0}{\leftarrow} \boldsymbol{\omega}_{\min}, \boldsymbol{\omega}_{iro} \underset{k=0}{\leftarrow} \boldsymbol{\omega}_{\max}, \tag{33}$$

where $[\boldsymbol{\omega}_{\min}, \boldsymbol{\omega}_{\max}]$ is the search space with respect to the parameter matrix $\boldsymbol{\omega}$.

4. Case studies

In this section, identification simulations using zigzag data based on the widely used KVLCC2 ship model and a fully-actuated Delfia 1* ship model in Delft University of Technology (Chen et al., 2019) are carried out to verify the modeling accuracy of the proposed ABEL method. Furthermore, the navigation data of a real model ship known as Tito-Neri tug ship (Haseltalab and Negenborn, 2019) is also used for identification experiments with real zigzag and free-running data. Several design parameters of the KVLCC2 model ship, Delfia 1* ship, and Tito-Neri model ship are shown in Table. 1 for reference.

Table 1: Several parameters of the KVLCC2 ship, Delfia 1* ship and Tito-Neri tug ship.

KVLCC2		Delfia 1*	TITO Neri
		Delfia 1* Propeller	Tito-Neri Propeller
Scale/(-)	1:45.7	1:16	1:30
Ship length/(m)	7	0.38	0.97
Moulded width/(m)	1.270	0.185	0.3
Moulded depth/(m)	0.656	0.07	0.18
Mass of the ship/(kg)	1908	3.345	16.9
Inertia moment/(kg.m^2)	1.027	0.031	0.51

4.1. Case study 1: Identifications based on KVLCC2 model

In this section, the KVLCC2 ship model is used for zigzag tests and identification simulations with different levels of disturbances and non-uniform sampling.

Table 2: Design parameters of the ABSAS, BSAS and LDWPSO.

Parameters	Common				ABSAS		LDWPSO		
	κ	n_{pop}	N	c	$s_{\min}$	η	c_1	c_2	w
Value	$\kappa_1 \sim \kappa_3 = 3$	4	20	1.1	10^-6	0.9	1.6	1.8	1-0.6*i/N
Significance	The normalization ratios	Population size	Maximum iteration	Constant	Minimum step	Attenuation coefficient	Learning factors		Velocity weight, i is the current iteration
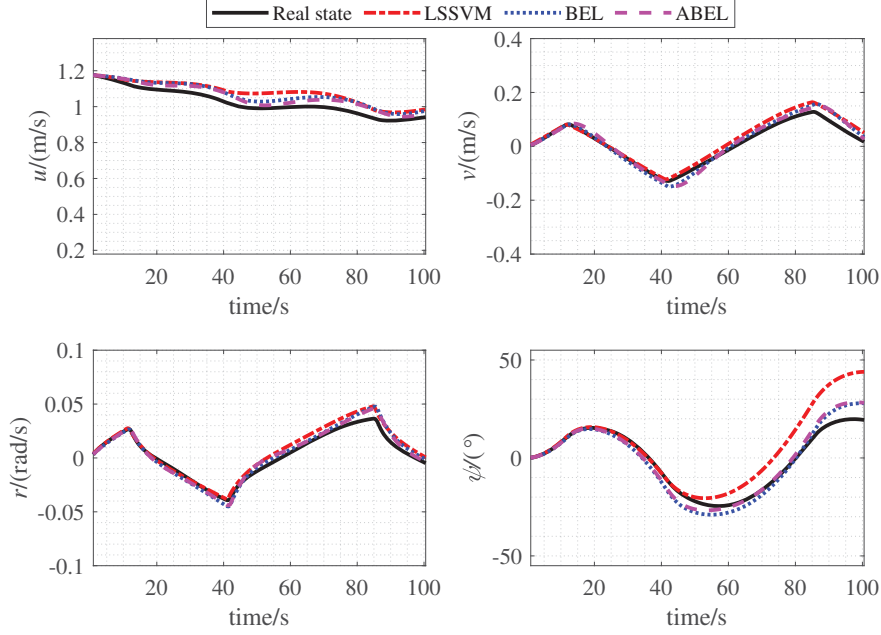
Figure 4: 10°/10° zigzag data regression results with no disturbances.

4.1.1. Identifications with different disturbances

Firstly, the 10°/10°, 20°/20° and 30°/30° zigzag simulation results of the KVLCC2 ship model without disturbances are applied for identification. After that, 30°/30° zigzag data with different levels of disturbances are selected to verify the effectiveness of ABEL. The traditional LSSVM method and original BSAS-optimized ESO-LSSVM, i.e., BEL, are both used as comparisons to analyze the influences of fine-tuning on the identification results. Besides, the normalization method is used to re-define the minimum and maximum values of the hyper-parameters as:

$$\omega[i] = \kappa_i \left(\mu'[i] - \mu'_{\min} \right) + \omega[i]_{\min},$$
$$\kappa_i = \frac{\omega[i]_{\max} - \omega[i]_{\min}}{\mu'_{\max} - \mu'_{\min}}, \tag{34}$$

where $\mu'_{\min} = -1$ and $\mu'_{\max} = 1$ are the normalized minimum and maximum values; κ_i is the ratio for the normalization of the ith dimension of the parameters μ. Then, the design parameters of the ABSAS and BSAS are set in Table 2.

(1) Identifications without disturbances

1) The identification results

The mean square errors (MSEs) of the predictions are used as the indicators of the identification. The prediction results of 10°/10°, 20°/20° and 30°/30° zigzag data based on the models identified by the proposed ABEL, BEL
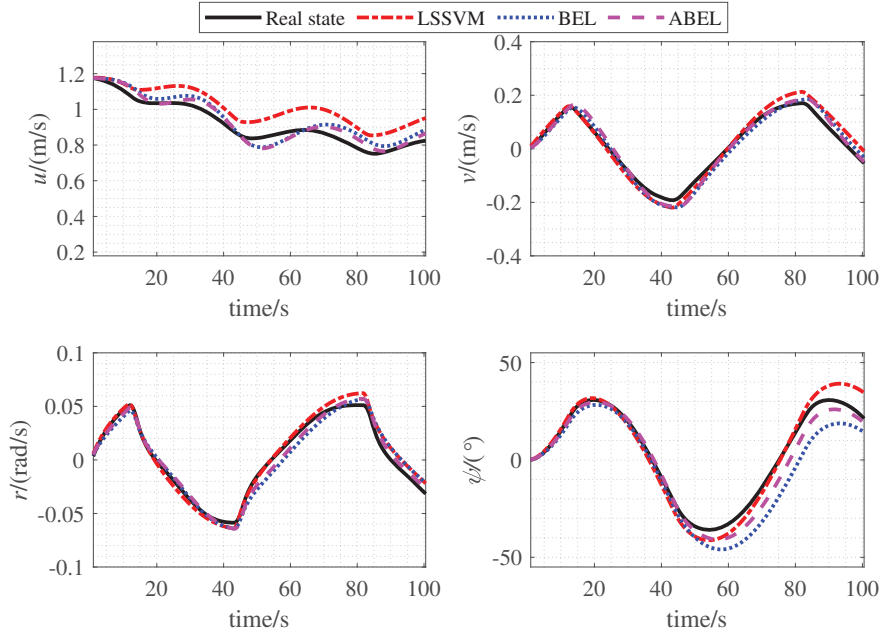
Figure 5: 20°/20° zigzag data regression results with no disturbances.
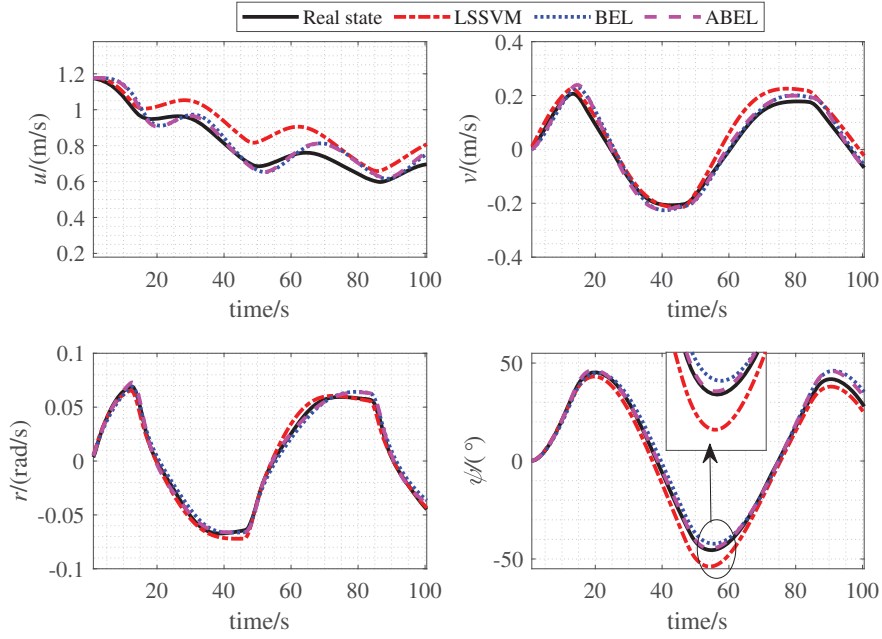

Figure 6: 30°/30° zigzag data regression results with no disturbances.

and traditional LSSVM are shown in Fig. 4~Fig. 6. The MSE results of the predicted states in 3-DOF are shown in Table 3. Besides, the detailed identified parameters of $\mathbf{\Theta}$ based on the 30°/30° zigzag data are shown in Table 4.

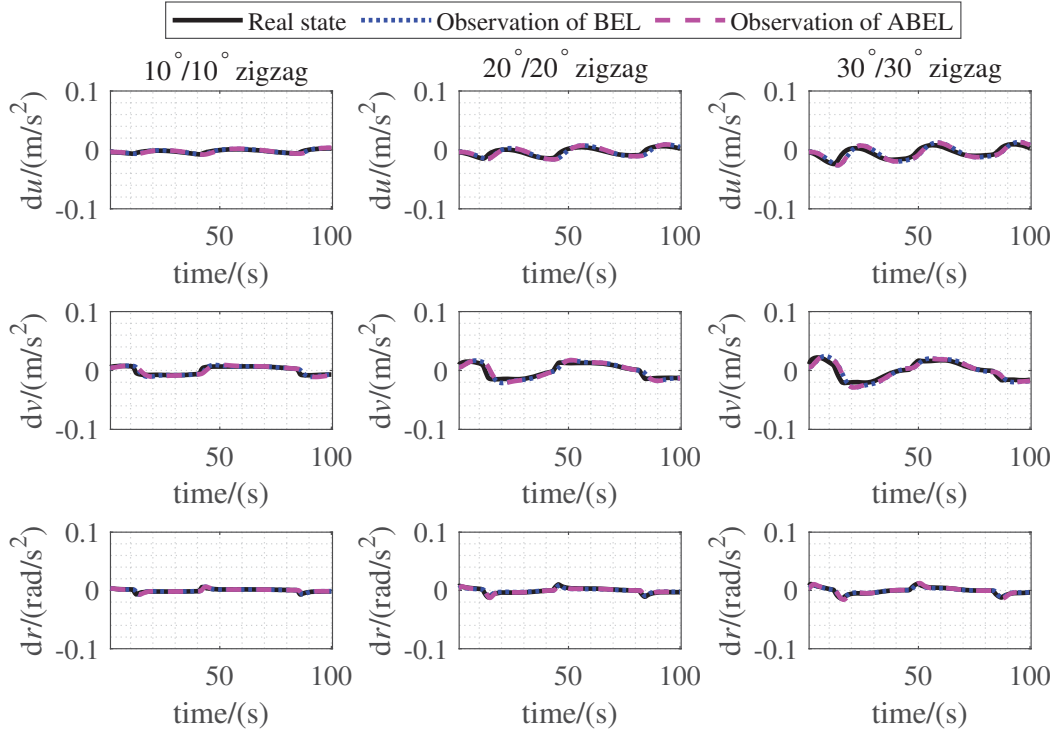The differential states are used for comparisons with the observation results, which are shown in Fig. 7. It can

Figure 7: ESO observation results of 10°/10°, 20°/20° and 30°/30° zigzag data with no disturbances.

Table 3: The prediction errors without disturbances.

Identification MSE	10°/10°			20°/20°			30°/30°		
	ABEL	BEL	LSSVM	ABEL	BEL	LSSVM	ABEL	BEL	LSSVM
u	1.16E-03	1.93E-03	3.46E-03	1.19E-03	2.02E-03	9.63E-03	1.63E-03	1.78E-03	9.95E-03
v	3.34E-04	2.83E-04	4.81E-04	4.09E-04	5.06E-04	7.15E-04	4.23E-04	4.36E-04	1.39E-03
r	1.77E-05	2.06E-05	3.37E-05	2.40E-05	5.30E-05	3.32E-05	7.89E-06	1.77E-05	1.60E-05
Fitness	1.61E-03	2.36E-03	4.18E-03	1.77E-03	2.90E-03	1.06E-02	2.10E-03	2.34E-03	1.15E-02

be seen that both the ESOs in ABEL and BEL can observe the higher-order states effectively. From the actual prediction results in Fig. 4~Fig. 6 and the MSEs in Table 3, it can be seen that the proposed ABEL method can obtain more accurate predictions than BEL and original LSSVM without disturbances, especially in the surge speed u. The corresponding fitness results of the ABEL are also smaller than those of the BEL and LSSVM.

In addition, the ship motion has stronger nonlinearity with a larger rudder angle, i.e., 30°/30° zigzag, which brings difficulties in the identification. From Table 3, it can be seen that the prediction errors of the original LSSVM and ABEL almost have a gap of magnitude order in 30°/30° zigzag test (e.g., the MSE of v of the ABEL is 4.23×10^{-4} while that of the LSSVM is 1.39×10^{-3}). Besides, the differences between the identified parameters of the LSSVM and ABEL in 30°/30° zigzag test are much larger than those between the BEL and ABEL, which is consistent with the prediction results.

(2) Identifications with disturbances

The equivalent lumped disturbances can be expressed by the composition of random disturbances and sinusoidal

Table 4: Identified parameters with 30°/30° zigzag data.

Parameters	Θ_u			Θ_v			Θ_r		
	ABEL	BEL	LSSVM	ABEL	BEL	LSSVM	ABEL	BEL	LSSVM
1	-2.08E-02	-2.17E-02	-1.07E-02	-3.62E-02	-3.17E-02	-2.54E-02	-6.22E-02	-7.76E-02	-8.36E-02
2	-2.45E-02	-2.56E-02	-1.26E-02	-6.15E-03	-6.21E-03	9.77E-15	-1.43E-03	-1.38E-03	-7.44E-15
3	-2.89E-02	-3.14E-02	-1.40E-03	-3.84E-02	-3.79E-02	-1.62E-02	-1.34E-02	-1.30E-02	2.28E-03
4	1.56E-02	1.79E-02	9.29E-03	-5.14E-02	-4.96E-02	-2.70E-02	-2.53E-02	-2.47E-02	-4.50E-04
5	-6.35E-01	-6.54E-01	-3.06E-01	-4.27E-02	-3.74E-02	-2.99E-02	7.63E-03	1.21E-02	3.84E-03
6	-7.69E-02	-7.23E-02	-4.86E-02	4.46E-01	4.33E-01	7.26E-02	-7.34E-02	-9.15E-02	-9.86E-02
7	-1.73E-07	-6.19E-07	4.16E-07	4.11E-04	4.09E-04	6.30E-04	3.94E-04	4.04E-04	3.36E-04
8	8.81E-08	-3.23E-07	-1.17E-06	-1.30E-03	8.99E-03	-1.47E-01	-1.39E-01	-1.12E-01	-8.36E-02
9	-2.56E-01	-2.49E-01	-1.45E-01	-2.68E-08	-3.51E-08	-5.83E-08	-6.74E-08	-8.73E-08	-5.29E-08
10	7.83E-04	9.59E-04	-1.23E-03	6.24E-03	8.74E-03	-3.62E-02	-3.55E-02	-2.97E-02	-2.10E-02
11	2.01E-03	2.30E-03	-8.83E-04	-4.91E-03	-5.76E-03	-6.77E-03	9.02E-04	-4.26E-04	-2.20E-03
12	-	-	-	-9.37E-06	-8.62E-06	3.06E-05	1.80E-06	1.14E-05	2.63E-05
13	-	-	-	6.50E-04	4.82E-04	5.92E-04	7.25E-04	5.61E-04	8.92E-05
14	-	-	-	1.59E-01	1.71E-01	5.13E-02	-4.09E-03	-1.83E-03	3.59E-03
15	-	-	-	-3.21E-03	8.14E-04	-2.04E-03	1.43E-02	1.09E-02	9.65E-03
16	-	-	-	-5.32E-05	-2.94E-04	-3.53E-05	8.46E-04	5.98E-04	-1.21E-04

Table 5: The prediction errors with different levels of disturbances.

Identification MSE	$f = 0.01$			$f = 0.02$			$f = 0.03$		
	ABEL	BEL	LSSVM	ABEL	BEL	LSSVM	ABEL	BEL	LSSVM
u	2.87E-03	3.69E-03	1.77E-02	1.19E-03	2.02E-03	9.63E-03	4.51E-03	1.00E-02	4.85E-02
v	5.55E-04	6.93E-04	1.33E-03	4.09E-04	5.06E-04	7.15E-04	6.15E-04	2.81E-03	1.32E-03
r	1.71E-05	2.46E-05	1.35E-04	2.40E-05	5.30E-05	3.32E-05	7.15E-05	4.54E-04	2.04E-04
Fitness	3.54E-03	4.55E-03	2.00E-02	1.77E-03	2.90E-03	1.06E-02	5.62E-03	1.60E-02	5.13E-02

periodic disturbances:

$$\boldsymbol{d}_i = F_i \left(\sin \left(\omega_d i + \theta_d \right) + 2r_d - 1 \right),$$
$$F_i = f_d \left| \boldsymbol{x}_i \right|, \tag{35}$$

where $\boldsymbol{d}_i$ is the setting disturbance for i^{th} sample; F_i is the amplitude of the disturbance, which is related to the absolute value of the states $\boldsymbol{x}_i$; f_d is the amplitude factor, which represent the relative level of the disturbances; ω_d and θ_i is the frequency and phase shift, respectively; r_d is a random value. In this case study, $\omega_d = 0.3\pi$ and $\theta_i = 0$ are set, and different amplitude factor $f_d = 0.01, 0.02$ and 0.03 are taken to verify the identification performance. The observation results and prediction results with the identified models are shown in Fig. 8~Fig. 10, and the final prediction MSEs are calculated as shown in Table 5.

It can be seen from the observation results in Fig. 8~Fig. 10 that the high-order differential states fluctuate obviously, while the states observed by the ESOs in ABEL and BEL are much smoother. The prediction results in Fig. 8~Fig. 10 also show that the predictions of the ABEL and BEL are more accurate than those of the traditional LSSVM in all cases, which indicates the effectiveness of the ESO-LSSVM scheme.

Besides, with the increase of f_d, under-fitting ($\dot{r}$ with $f_d = 0.02$) or over-fitting ($\dot{v}$ with $f_d = 0.03$) problems occur in the observations of BEL. On one hand, the BEL has larger observation errors on the over-shots of $\dot{r}$ as shown in Fig. 9, thus the prediction error of r of the BEL (5.30×10^{-5}) is larger than those of the proposed ABEL (2.40×10^{-5}), respectively. On the other hand, the BEL has an over-fitting problem in the observation of $\dot{v}$ as shown in Fig. 10,
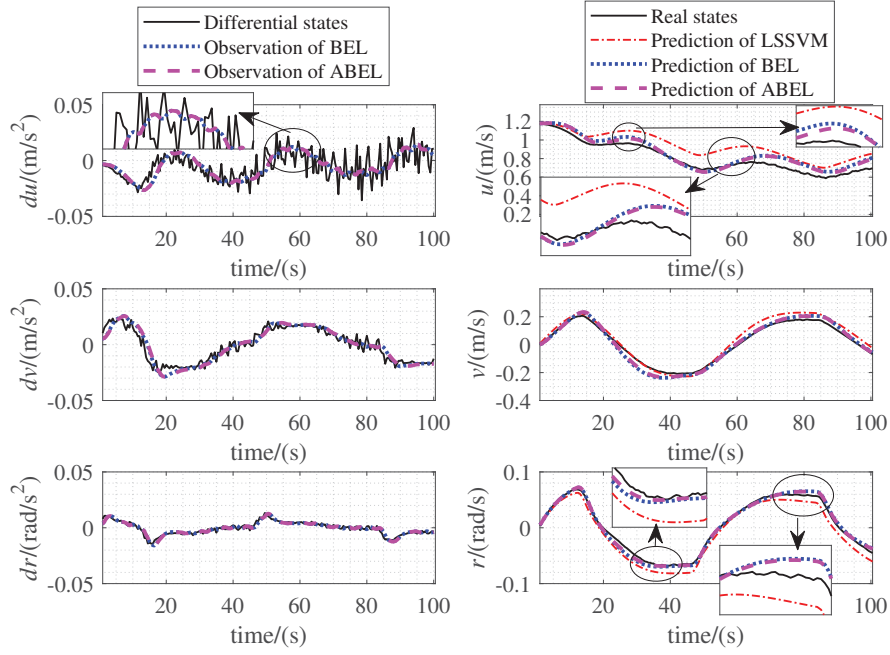
Figure 8: ESO observation results and prediction results of 30°/30° zigzag data with $f_d = 0.01$.
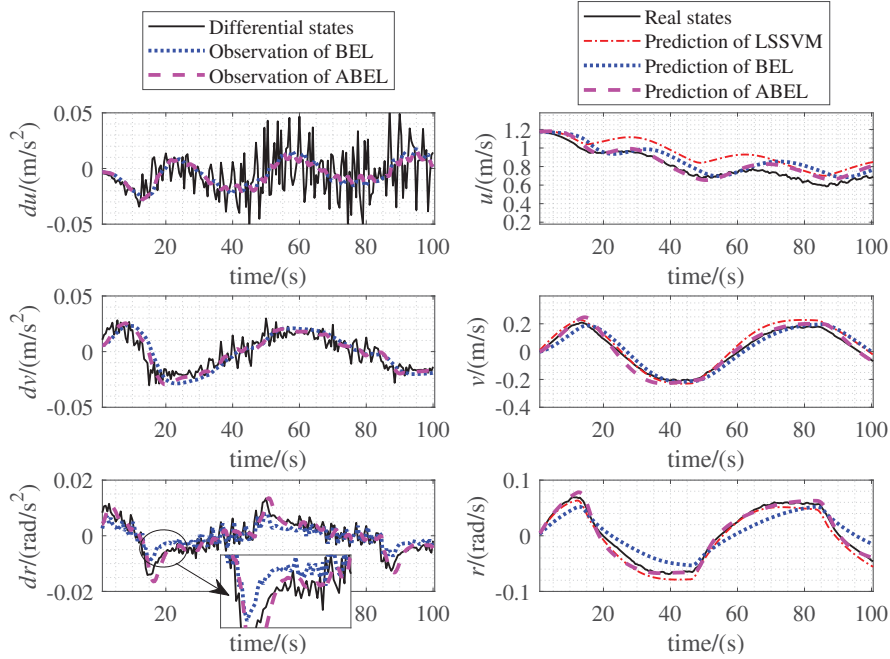

Figure 9: ESO observation results and prediction results of 30°/30° zigzag data with $f_d = 0.02$.

which results in unsmooth observations. Therefore, the final prediction error of v (2.81×10^{-3}) is still larger than that of the ABEL (6.15×10^{-4}).

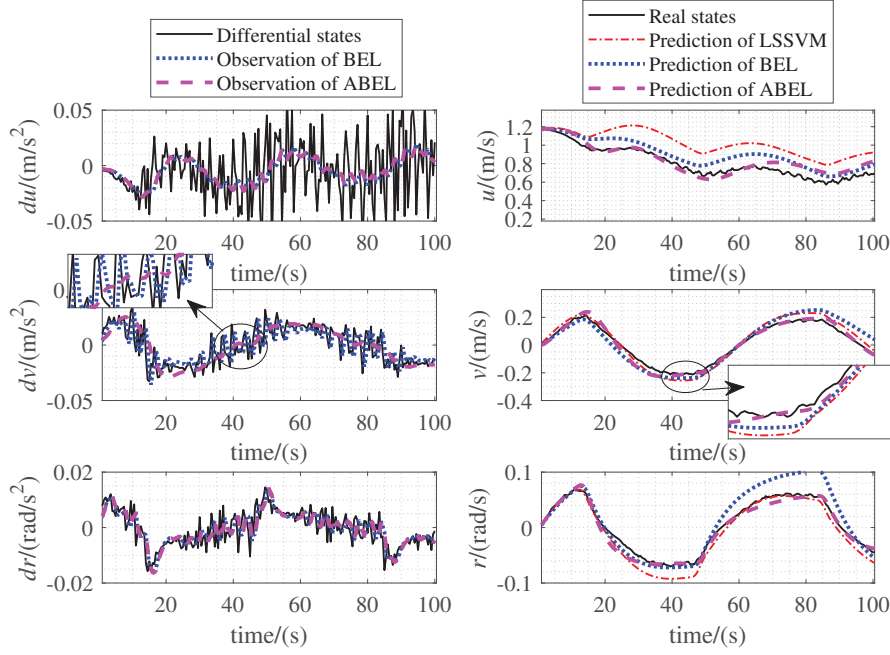In summary, the identification results with different levels of disturbances indicate that both the proposed ABEL

Figure 10: ESO observation results and prediction results of $30°/30°$ zigzag data with $f_d = 0.03$.

and original BSAS-optimized ESO-LSSVM (BEL) can obtain better identification results than traditional LSSVM method. Besides, the proposed ABEL outperforms the BEL, which shows the effectiveness of the fine-tuning for ESO-LSSVM.

4.1.2. Identifications with non-uniform sampling

In data acquisition, sampling loss is typical reason of non-uniform sampling. In this case, the non-uniform sampling is realized by randomly removing a certain proportion λ_s of the samples. The identification experiments with $\lambda_s = 10\%$, 20% and 30% are carried out respectively. The observation results and prediction results are shown in Fig. 11~Fig. 13. The prediction MSEs are shown in Table 6.

Table 6: The prediction errors with non uniform sampling.

Identification	$\lambda_s = 10\%$			$\lambda_s = 20\%$			$\lambda_s = 30\%$		
RMSE	ABEL	BEL	LSSVM	ABEL	BEL	LSSVM	ABEL	BEL	LSSVM
u	4.61E-03	1.61E-02	2.62E-02	1.42E-03	2.00E-03	5.49E-03	2.87E-03	9.75E-03	6.38E-02
v	7.36E-04	2.11E-03	1.86E-03	4.47E-04	3.76E-04	2.03E-03	9.30E-04	2.04E-03	3.12E-02
r	2.86E-05	1.06E-04	2.00E-04	4.15E-05	5.51E-05	1.85E-04	5.37E-05	3.19E-04	3.18E-04
Fitness	5.55E-03	1.89E-02	2.95E-02	2.15E-03	2.76E-03	8.82E-03	4.17E-03	1.40E-02	9.72E-02

From Fig. 11~Fig. 13, it can be observed that the non-uniform sampling also has influences on the final identification results. Benefiting from the observations of ESOs, the proposed ABEL and BEL method can obviously obtain better prediction results than the traditional LSSVM, especially in the prediction of u, which indicates the ESO-LSSVM scheme can handle with the non-uniform sampling problem as expected. In addition, it can be seen from Table 6, the proposed ABEL obtains the smallest fitness results and the errors of the predicted states in most of
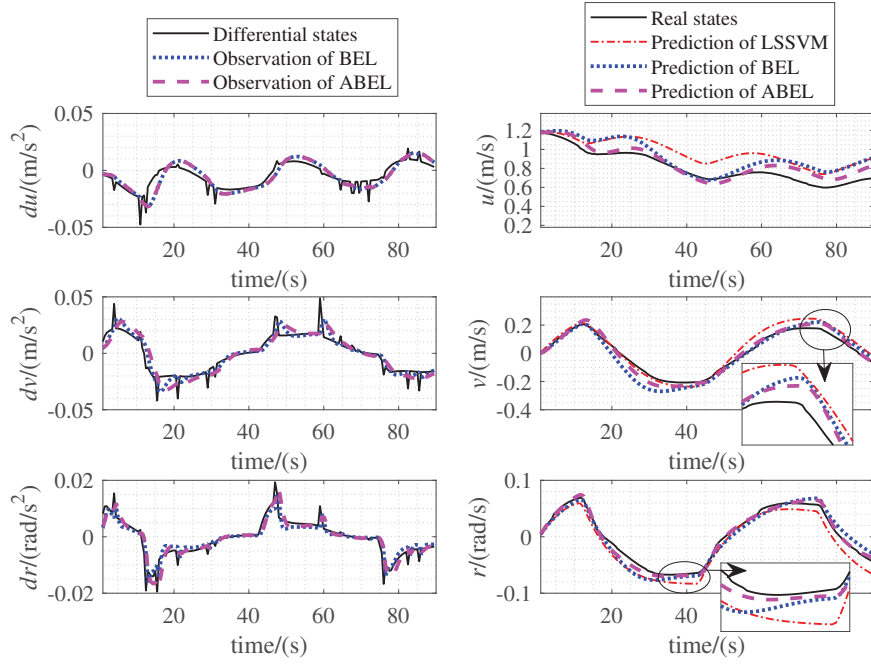
19

Figure 11: ESO observation results and prediction results of $30°/30°$ zigzag data with $\lambda_s = 10\%$.

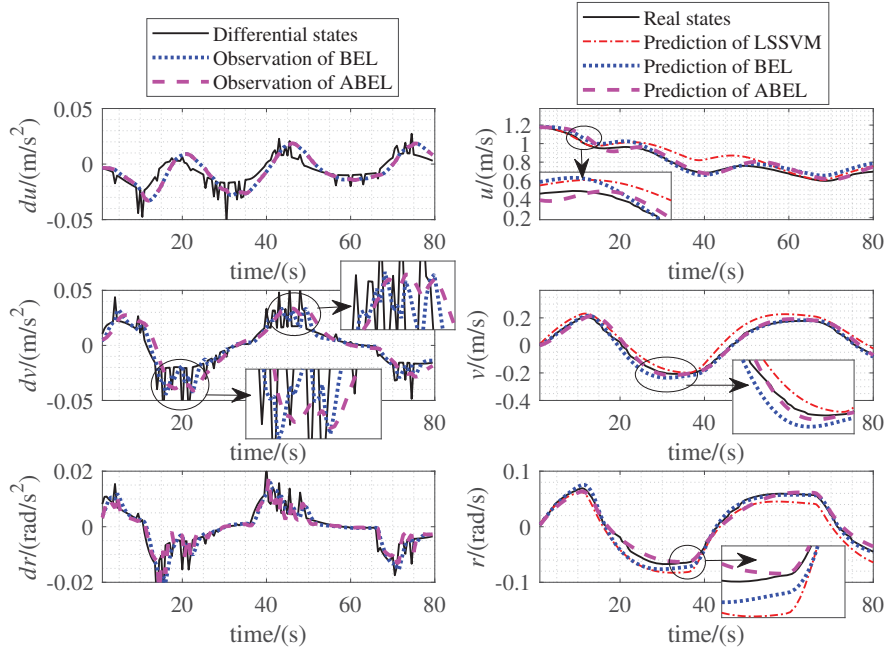Figure 12: ESO observation results and prediction results of $30°/30°$ zigzag data with $\lambda_s = 20\%$.

the cases, expect that the MSE of v with $\lambda_s = 20\%$ is a bit larger than that of the BEL.

Therefore, it can be concluded that the proposed method also outperforms the BEL and traditional LSSVM methods with non-uniform sampling disturbances.
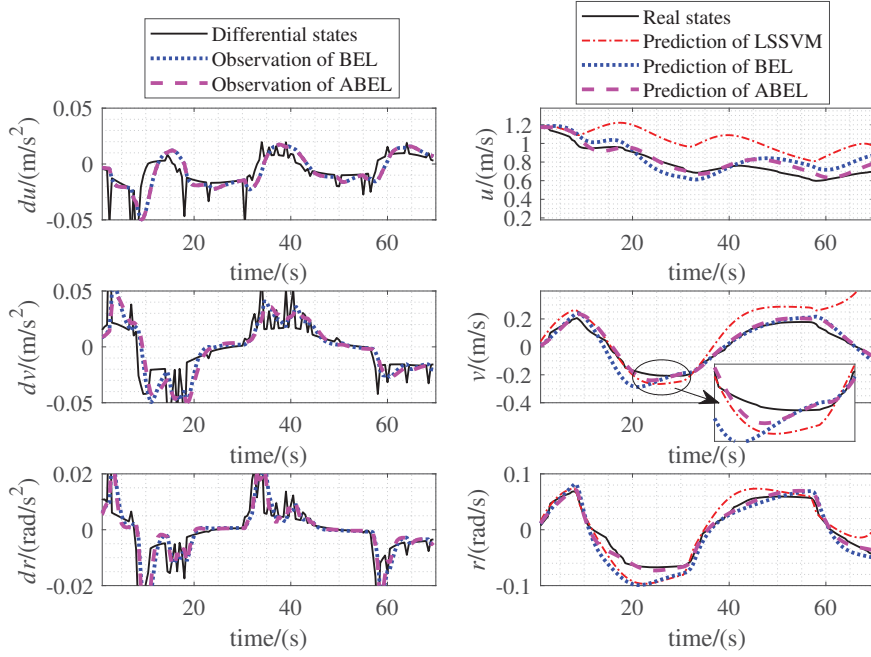
20

Figure 13: ESO observation results and prediction results of 30°/30° zigzag data with $\lambda_s = 30\%$.

4.2. Case study 2: Identifications based on Delfia 1* ship model

Delfia 1* ship has two 360° steering propellers, which can make maneuvering applications in crowded environments by flexible steering with large rudder angles. In this section, 50°/50° zigzag tests are conducted based on the Delfia 1* ship model to verify the modeling performance of the proposed ABEL with large nonlinearities. The zigzag data with different levels of uncertain disturbances ($f_d = 0.01$ and $f_d = 0.04$) and non-uniform sampling ($\lambda_s = 10\%$ and $\lambda_s = 40\%$) are both considered for identification.

Table 7: The prediction errors of Delfia 1*.

Zigzag	MSE	$f_d = 0.01$			$f_d = 0.04$		
		ABEL	BEL	LSSVM	ABEL	BEL	LSSVM
	u	8.60E-04	8.67E-04	1.27E-02	9.76E-03	9.86E-03	7.51E-01
	v	2.34E-04	3.27E-04	5.96E-04	8.89E-04	7.31E-04	4.38E-02
Uncertain disturbances	r	4.42E-04	6.44E-04	4.00E-03	4.54E-03	1.03E-02	3.40E-01
	Fitness	1.26E-03	1.44E-03	1.48E-02	1.24E-02	1.25E-02	9.24E-01
Zigzag	MSE	$\lambda_s = 10\%$			$\lambda_s = 40\%$		
		ABEL	BEL	LSSVM	ABEL	BEL	LSSVM
	u	5.77E-05	1.49E-04	1.72E-02	1.87E-04	3.61E-04	6.22E-02
	v	2.82E-05	5.12E-05	1.14E-03	1.47E-04	1.38E-04	1.27E-03
Non-uniform sampling	r	5.27E-04	6.08E-04	7.09E-03	1.98E-03	2.15E-03	1.62E-02
	Fitness	2.86E-04	4.31E-04	2.10E-02	1.09E-03	1.32E-03	6.96E-02

The observation results and prediction results with uncertain disturbances are shown in Fig. 14 and Fig. 15 and the results with non-uniform sampling are shown in Fig. 16 and Fig. 17. The prediction MSEs are shown in Table 7.

From the prediction errors in Table 7, it can be observed that the proposed ABEL and BEL methods can obtain
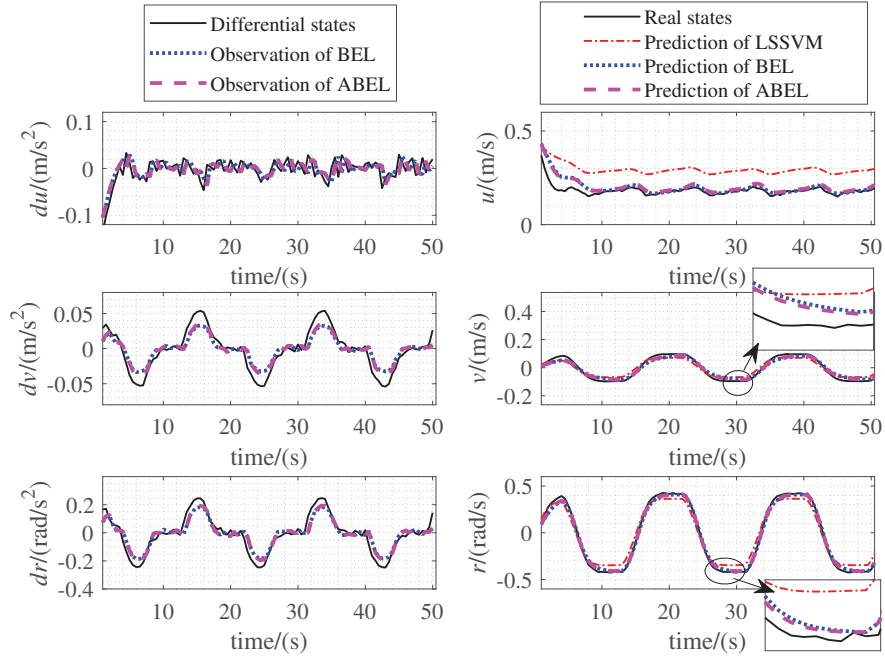
21

Figure 14: ESO observation results and prediction results of $50°/50°$ zigzag data with $f_d = 0.01$.

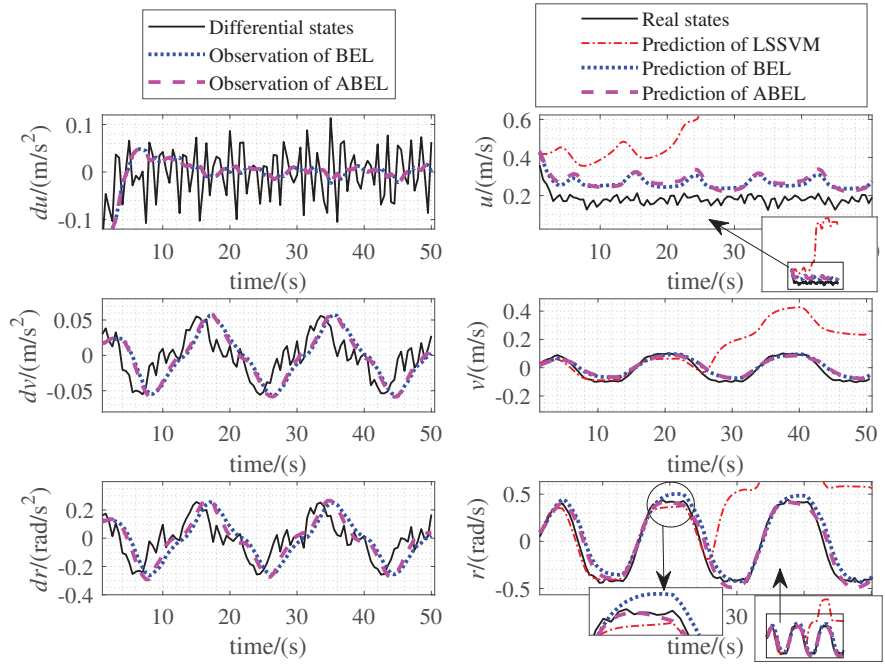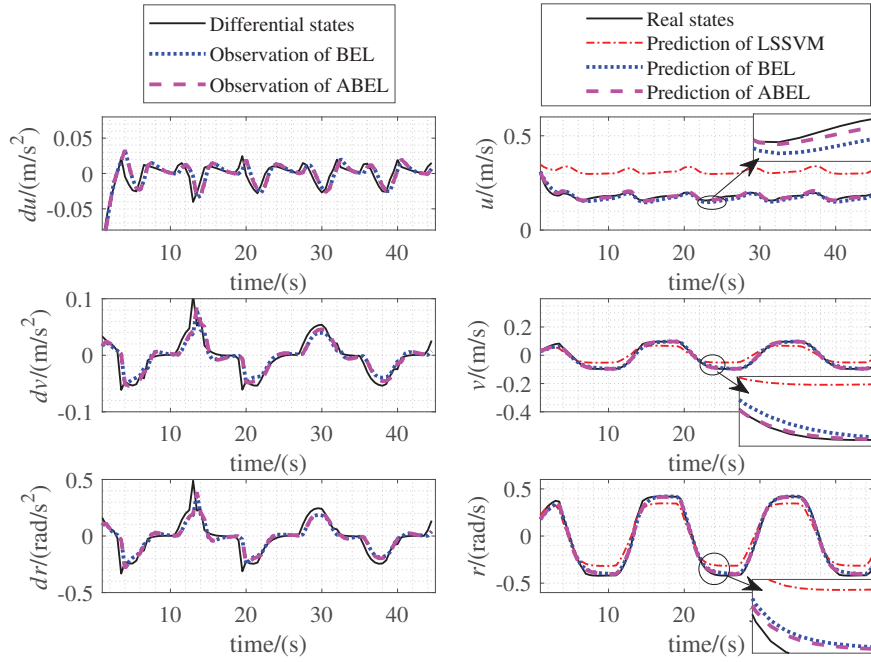Figure 15: ESO observation results and prediction results of $50°/50°$ zigzag data with $f_d = 0.04$.

smaller prediction errors of both u, v and r (especially u and r) than the traditional LSSVM under different levels of disturbances and non-uniform sampling. Particularly, as can be seen from Fig. 15, the predicted results of u and v by the traditional LSSVM deviate greatly from the actual values due to the strong random disturbances with $f_d = 0.4$. In

22

Figure 16: ESO observation results and prediction results of $50°/50°$ zigzag data with $\lambda_s = 10\%$.
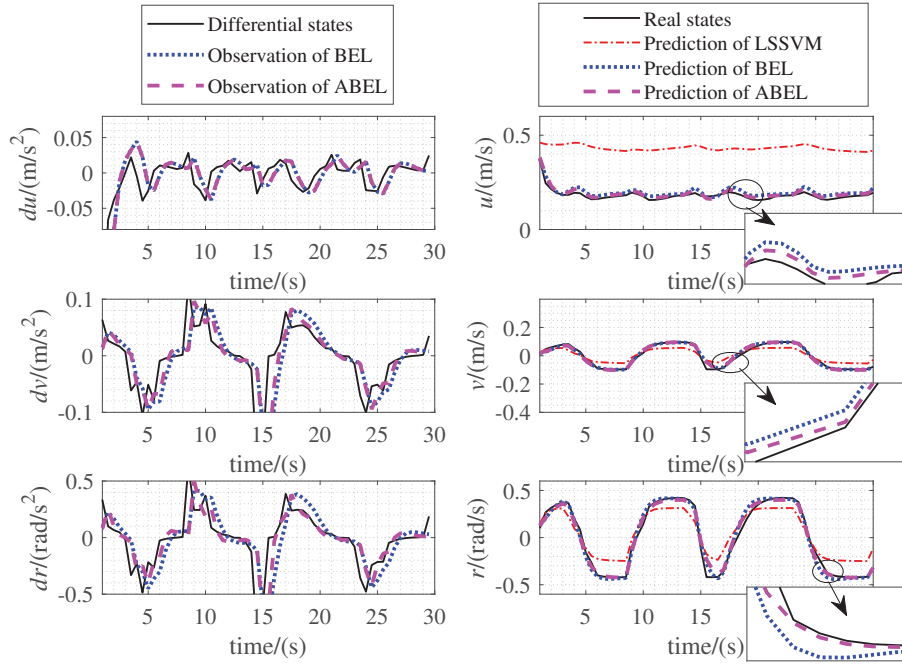
Figure 17: ESO observation results and prediction results of $50°/50°$ zigzag data with $\lambda_s = 40\%$.

spite of this, the proposed ABEL and BEL can still predict the u and v accurately, which indicates the effectiveness of the ESO-LSSVM scheme.

Besides, compared with BEL, the proposed ABEL can obtain more accurate state predictions in most of the cases.

23

Moreover, the final fitness results in the proposed ABEL in all cases are better than those in BEL, which verifies the optimization performance of the proposed ABSAS algorithm.

4.3. Case study 3: Identifications based on real test data of Tito-Neri ship

In addition to the standard zigzag data, the free-sailing data during the voyage are also usually used for identification. We collect real test data of the Tito-Neri ship when sailing in the open pool in Delft University of Technology (52°00'08.1"N, 4°22'17.2"E) as shown in Fig. 18.

Figure 18: Sailing data collection of Tito-Neri ship in the open pool in Delft University of Technology.
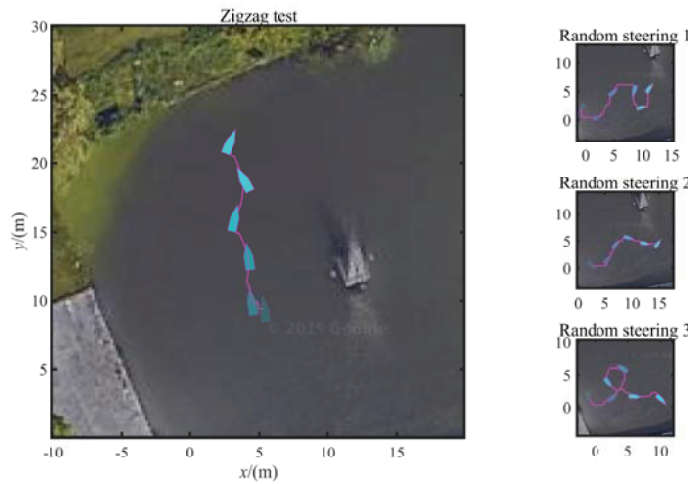

Figure 19: The trajectories generated by random steering of Tito-Neri ship.

A remote control software is developed by Python to control the ship and collect the real-time data of Tito-Neri through wireless communication, which can also use a joystick to control the ship in free-sailing mode. The GPS and IMU sensors are installed on Tito-Neri for acquiring the position and attitude states. The proposed ABEL and original LSSVM methods are used for identification modeling based on the collected data. The standard 20°/20° zig-zag test data and the random steering data of Tito-Neri are both collected for identification modeling. The trajectories
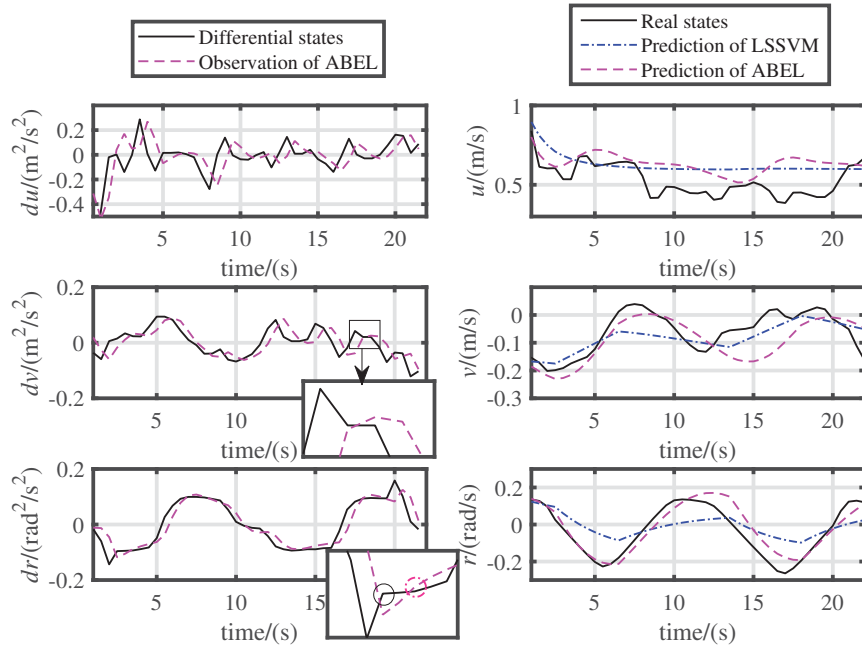
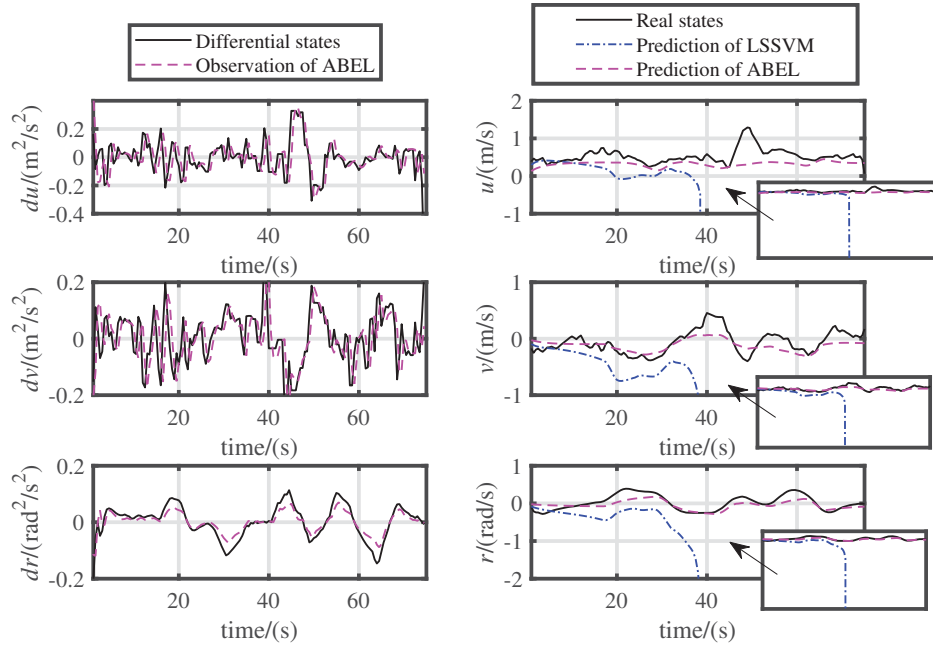Figure 20: The prediction results of real 20°/20° zigzag data of Tito-Neri ship.

Figure 21: The prediction results of sample 1.

generated by random steering are shown in Fig. 19. The prediction results of the surge, sway and yaw velocities of all samples are shown in Fig. 20~Fig. 23 and the prediction errors are calculated as shown in Table 8.

Due to the disturbances and uncertainties in measurements of the GPS and IMU sensors, the real data of Tito-Neri
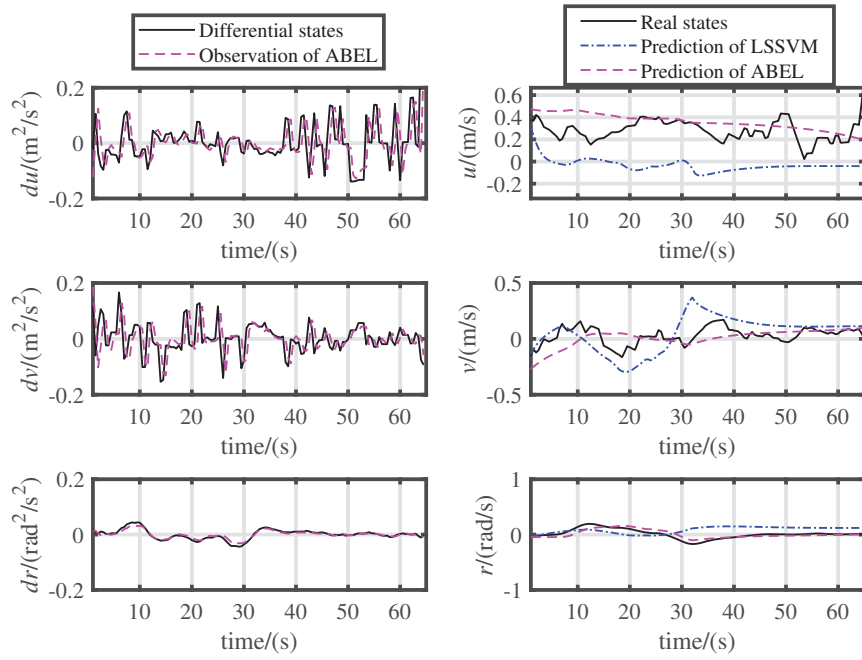
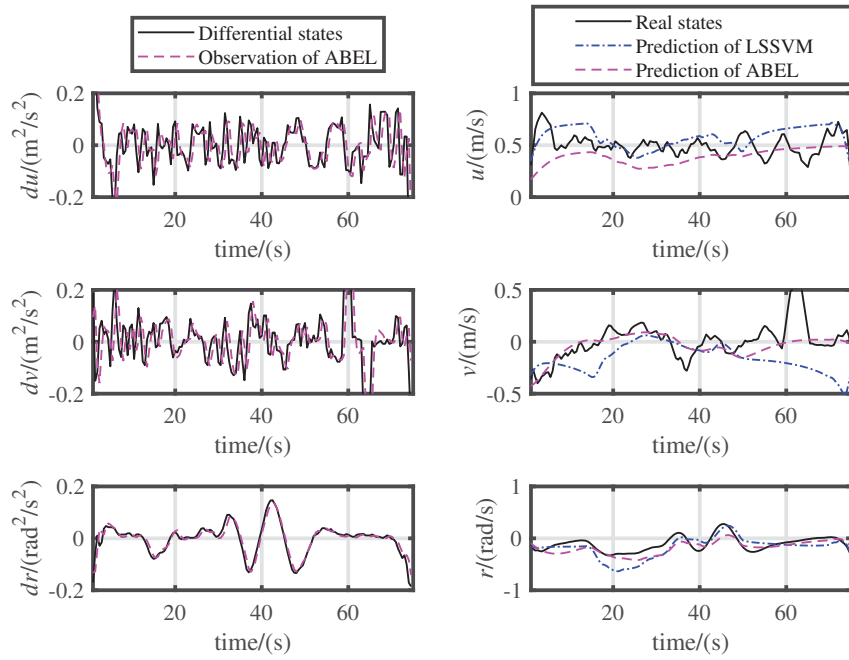Figure 22: The prediction results of sample 2.

Figure 23: The prediction results of sample 3.

model ship contains irregularities. In spite of this, it can be seen from the prediction results that the proposed ABEL method can predict the ship motion states in both the zigzag test and random steering tests, while the original LSSVM fails to modeling an effective ship model in random steering test 1 as in Fig. 21 and obtains much higher prediction

Table 8: The prediction errors of real test data

MSE	Zigzag				Sample 1			
	u	v	r	Fitness	u	v	r	Fitness
ABEL	1.93E-02	4.33E-03	3.05E-03	2.59E-01	7.76E-02	2.27E-02	1.84E-02	5.62E-01
LSSVM	1.97E-02	8.71E-03	1.81E-02	3.65E-01	1.62E+03	3.33E+12	1.03E+13	4.98E+06

MSE	Sample 2				Sample 3			
	u	v	r	Fitness	u	v	r	Fitness
ABEL	2.13E-02	1.01E-02	2.21E-03	2.93E-01	1.86E-02	1.93E-02	1.05E-02	3.76E-01
LSSVM	7.70E-02	6.20E-03	9.64E-03	4.52E-01	2.32E-02	6.09E-02	2.24E-02	5.46E-01

errors than the proposed method in all tests as shown in Table 8. Moreover, as can be seen from the amplified figures in Fig. 20, the ESO in the proposed method can generate smoother observations for the identification, which results in a higher identification accuracy.

In summary, it can be concluded from the above case studies that the proposed ABEL can obtain more accurate ship motion models than the traditional LSSVM with different levels of disturbances and non-uniform sampling, by reasonable exploitation of the ESO observations and optimization of the ABSAS algorithm.

5. Conclusions and future research

In this study, in order to obtain an accurate ship model with uncertain disturbances and non-uniform sampling, a novel ABEL identification method is proposed by combining an ESO, LSSVM and an ABSAS optimizer. The observations of the higher-order states in ESO are used instead of the actual measurements with disturbances. The hyper-parameter of ESO are fine-tuned by the ABSAS optimizer. The following conclusions are drawn from several identification cases studies:

(1) In terms of the identification performance, with different levels of disturbances and non-uniform sampling, the proposed method can obtain more accurate modeling results than the traditional LSSVM method, which shows the effectivenesses of the proposed ESO-LSSVM scheme.

(2) In terms of the fine-tuning performance, the identification results show that the integrating ABSAS performs better than the original BSAS, which results in better identification results. Therefore, appropriate hyper-parameters of the ESO are important for the optimal identification of the proposed method.

With the diversification of ship types and the requirement of autonomous collision avoidance, the ship maneuverability will change with the speed during the voyage, which requires on-line identification. Hence, the implementation of the proposed method in on-line identification will be studied in future research.

Acknowledgements

References

Abkowitz, M. A., 1980. Measurement of hydrodynamic characteristics from ship maneuvering trials by system identification. Tech. rep.

Ahmed-Ali, T., Kenné, G., Lamnabhi-Lagarrigue, F., 2009. Identification of nonlinear systems with time-varying parameters using a sliding-neural network observer. Neurocomputing 72 (7-9), 1611–1620.

Bai, W., Ren, J., Li, T., 2018. Multi-innovation gradient iterative locally weighted learning identification for a nonlinear ship maneuvering system. China Ocean Engineering 32 (3), 288–300.

Bai, W., Ren, J., Li, T., 2019a. Modified genetic optimization-based locally weighted learning identification modeling of ship maneuvering with full scale trial. Future Generation Computer Systems 93, 1036–1045.

Bai, W., Ren, J., Li, T., Chen, C. P., 2019b. Grid index subspace constructed locally weighted learning identification modeling for high dimensional ship maneuvering system. ISA transactions 86, 144–152.

Bonnabel, S., Mirrahimi, M., Rouchon, P., 2009. Observer-based hamiltonian identification for quantum systems. Automatica 45 (5), 1144–1155.

Chen, L., Huang, Y., Zheng, H., Hopman, J. J., Negenborn, R., 2019. Cooperative multi-vessel systems in urban waterway networks. IEEE Transactions on Intelligent Transportation Systems (1), 1–14.

Cui, R., Chen, L., Yang, C., Chen, M., 2017. Extended state observer-based integral sliding mode control for an underwater robot with unknown disturbances and uncertain nonlinearities. IEEE Transactions on Industrial Electronics 64 (8), 6785–6795.

Fossen, T. I., Sagatun, S. I., Sørensen, A. J., 1996. Identification of dynamically positioned ships. Control Engineering Practice 4 (3), 369–376.

Gao, Z., 2006. Scaling and bandwidth-parameterization based controller tuning. In: Proceedings of the American control conference. Vol. 6. pp. 4989–4996.

Guo, Q., Zhang, Y., Celler, B. G., Su, S. W., 2016. Backstepping control of electro-hydraulic system based on extended-state-observer with plant dynamics largely unknown. IEEE Transactions on industrial Electronics 63 (11), 6909–6920.

Haseltalab, A., Negenborn, R. R., 2019. Model predictive maneuvering control and energy management for all-electric autonomous ships. Applied Energy 251, 113308.

Haseltine, E. L., Rawlings, J. B., 2005. Critical evaluation of extended Kalman filtering and moving-horizon estimation. Industrial & engineering chemistry research 44 (8), 2451–2460.

Hou, X.-R., Zou, Z.-J., 2015. SVR-based identification of nonlinear roll motion equation for FPSOs in regular waves. Ocean Engineering 109, 531–538.

Hou, X.-R., Zou, Z.-J., Liu, C., 2018. Nonparametric identification of nonlinear ship roll motion by using the motion response in irregular waves. Applied Ocean Research 73, 88–99.

Ikeda, K., Mogami, Y., Shimomura, T., 2003. Continuous-time model identification by using adaptive observer. IFAC Proceedings Volumes 36 (16), 309–314.

Jiang, X., Li, S., 2018. BAS: Beetle antennae search algorithm for optimization problems. International Journal of Robotics and Control 1 (1), 1–5.

Kawan, B., Wang, H., Li, G., Chhantyal, K., 2017. Data-driven modeling of ship motion prediction based on support vector regression. In: Proceedings of the Linkping Electronic Conference. pp. 350–354.

Li, M. W., Geng, J., Han, D. F., Zheng, T. J., 2016. Ship motion prediction using dynamic seasonal RvSVR with phase space reconstruction and the chaos adaptive efficient FOA. Neurocomputing 174 (4), 661–680.

Lin, M., Li, Q., 2018. A hybrid optimization method of beetle antennae search algorithm and particle swarm optimization. DEStech Transactions on Engineering and Technology Research (ecar).

Lin, X., Liu, Y., Wang, Y., 2018. Design and research of DC motor speed control system based on improved BAS. In: 2018 Chinese Automation Congress (CAC). IEEE, pp. 3701–3705.

Liu, C., Negenborn, R. R., Zheng, H., Chu, X., 2017a. A state-compensation extended state observer for model predictive control. European Journal of Control 36, 1–9.

Liu, H., Jiang, G.-P., Fan, C.-X., 2008. State-observer-based approach for identification and monitoring of complex dynamical networks. In: APCCAS 2008-2008 IEEE Asia Pacific Conference on Circuits and Systems. IEEE, pp. 1212–1215.

Liu, H., Li, S., 2011. Speed control for PMSM servo system using predictive functional control and extended state observer. IEEE Transactions on Industrial Electronics 59 (2), 1171–1183.

Liu, R., Nie, Z., Hui, S., Yan, L., Zheng, Y., 2017b. Identification for hysteresis nonlinear system based on extended state observer. Chinese Journal of Scientific Instrument 38 (8), 1970–1977.

Luo, W., 2009. On the modeling of ship manoeuvring motion by using support vector machines. Ph.D. thesis, Shanghai Jiao Tong University.

Luo, W., Li, X., 2017. Measures to diminish the parameter drift in the modeling of ship manoeuvring using system identification. Applied Ocean Research 67, 9–20.

Luo, W., Soares, C. G., Zou, Z., 2016. Parameter identification of ship maneuvering model based on support vector machines and particle swarm optimization. Journal of Offshore Mechanics and Arctic Engineering 138 (3), 031101.

Ma, X., Ding, F., 2015. Gradient-based parameter identification algorithms for observer canonical state space systems using state estimates. Circuits, Systems, and Signal Processing 34 (5), 1697–1709.

Nie, Z., Guo, D., Liu, R., 2017. Parameter identification for adjustable systems based on extended state observer and experimental study. Control and Decision 32 (10), 1905–1909.

Pablo, M., Bossio, G. R., Solsona, J. A., García, G. O., 2008. On-line iron loss resistance identification by a state observer for rotor-flux-oriented control of induction motor. Energy conversion and management 49 (10), 2742–2747.

Shao, X., Wang, H., 2015. Performance analysis on linear extended state observer and its extension case with higher extended order. Control and Decision 30 (5), 815–822.

Sheng, L., Na, J., 2009. SVM parameters optimization algorithm and its application. In: IEEE International Conference on Mechatronics & Automation.

Sonnenburg, C. R., Woolsey, C. A., 2013. Modeling, identification, and control of an unmanned surface vehicle. Journal of Field Robotics 30 (3), 371–398.

Su, J., Qiu, W., Ma, H., Woo, P.-Y., 2004. Calibration-free robotic eye-hand coordination based on an auto disturbance-rejection controller. IEEE Transactions on Robotics 20 (5), 899–907.

Sun, Y., Zhang, J., Li, G., Wang, Y., Sun, J., Jiang, C., 2019. Optimized neural network using beetle antennae search for predicting the unconfined compressive strength of jet grouting coalcretes. International Journal for Numerical and Analytical Methods in Geomechanics.

Suykens, J. A., Vandewalle, J., 1999. Least squares support vector machine classifiers. Neural processing letters 9 (3), 293–300.

Wang, J., Chen, H., 2018. BSAS: Beetle swarm antennae search algorithm for optimization problems. arXiv preprint arXiv:1808.00206.

Wang, T., Yang, L., Liu, Q., 2018. Beetle swarm optimization algorithm: Theory and application. arXiv preprint arXiv:1808.00206.

Wang, X.-g., Zou, Z.-j., Hou, X.-r., Feng, X., 2015. System identification modelling of ship manoeuvring motion based on support vector regression. Journal of Hydrodynamics, Ser. B 27 (4), 502–512.

Wu, Q., Lin, H., Jin, Y., Chen, Z., Li, S., Chen, D., 2019. A new fallback beetle antennae search algorithm for path planning of mobile robots with collision-free capability. Soft Computing, 1–12.

Xie, S., Chu, X., Liu, C., Liu, J., Mou, J., 2019a. Parameter identification of ship motion model based on multi-innovation methods. Journal of Marine Science and Technology, 1–23.

Xie, S., Chu, X., Liu, C., Zheng, M., 2019b. Marine diesel engine speed control based on adaptive state-compensate extended state observer-backstepping method. Proceedings of the Institution of Mechanical Engineers, Part I: Journal of Systems and Control Engineering 233 (5), 457–471.

Xie, S., Chu, X., Zheng, M., Liu, C., 2019c. Ship predictive collision avoidance method based on an improved beetle antennae search algorithm. Ocean Engineering 192, 106542.

Xie, S., Garofano, V., Chu, X., Negenborn, R. R., 2019d. Model predictive ship collision avoidance based on Q-learning beetle swarm antenna search and neural networks. Ocean Engineering 193, 106609.

Xu, L., Ding, F., Gu, Y., Alsaedi, A., Hayat, T., 2017. A multi-innovation state and parameter estimation algorithm for a state space system with d-step state-delay. Signal Processing 140, 97–103.

Yasukawa, H., Yoshimura, Y., 2015. Introduction of MMG standard method for ship maneuvering predictions. Journal of Marine Science and Technology 20 (1), 37–52.

Zhang, R., Han, J., 2000. Parameter identification by model compensation auto disturbance rejection controller. Control Theory & Applications 17 (1), 79–81.

Zhang, X., Zou, Z., 2011. Identification of Abkowitz model for ship manoeuvring motion using ε-support vector regression. Journal of Hydrodynamics 23 (3), 353–360.

Zhang, X., Zou, Z., 2013a. Black-box modeling of ship manoeuvring motion based on feed-forward neural network with Chebyshev orthogonal basis function. Journal of marine science and technology 18 (1), 42–49.

Zhang, X., Zou, Z., 2013b. Estimation of the hydrodynamic coefficients from captive model test results by using support vector machines. Ocean

Engineering 73, 25–31.

Zheng, H., Negenborn, R. R., Lodewijks, G., 2017. Fast ADMM for distributed model predictive control of cooperative waterborne AGVs. IEEE Transactions on Control Systems Technology 25 (4), 1406 – 1413.

Zheng, H., Negenborn, R. R., Lodewijks, G., 2018. Robust distributed predictive control of waterborne AGVsA cooperative and cost-effective approach. IEEE Transactions on Cybernetics 48 (8), 2449–2461.

Zhou, Y., Huang, Z., Li, H., Peng, J., Liu, W., Liao, H., 2018. A generalized extended state observer for supercapacitor state of energy estimation with online identified model. IEEE Access 6, 27706–27716.

Zhu, M., Hahn, A., Wen, Y., Bolles, A., 2017a. Parameter identification of ship maneuvering models using recursive least square method based on support vector machines. TransNav: International Journal on Marine Navigation and Safety of Sea Transportation 11.

Zhu, M., Hahn, A., Wen, Y.-Q., Bolles, A., 2017b. Identification-based simplified model of large container ships using support vector machines and artificial bee colony algorithm. Applied Ocean Research 68, 249–261.

Zhu, S., Zhu, D., Deng, Z., 2013. Identification of underwater vehicle dynamic model using multi-innovation least squares algorithm. Journal of System Simulation 25, 1399–1404.